JCS ePress online publication date 17 November 2009

Presenilin-1 acts via Id1 to regulate the function of muscle satellite cells in a γ-secretase-independent manner

Yusuke Ono[1,*], Viola F. Gnocchi[1], Peter S. Zammit[1,‡] and Ryoichi Nagatomi[2,‡]

[1]King's College London, Randall Division of Cell and Molecular Biophysics, Guy's Campus, London, SE1 1UL, UK
[2]Department of Medicine & Science in Sports & Exercise, Tohoku University Graduate School of Medicine, Sendai 980-8575, Japan
*Author for correspondence (yusuke.ono@kcl.ac.uk)
‡These authors contributed equally

Accepted 20 September 2009
Journal of Cell Science 122, 4427-4438 Published by The Company of Biologists 2009
doi:10.1242/jcs.049742

Summary

Muscle satellite cells are the resident stem cells of adult skeletal muscle. Here, we have examined the role of the multifunctional protein presenilin-1 (PS1) in satellite cell function. PS1 acts as a crucial component of the γ-secretase complex, which is required to cleave single-pass transmembrane proteins such as Notch and amyloid-β precursor protein. PS1, however, also functions through γ-secretase-independent pathways. Activation of satellite cells was accompanied by induction of PS1, with PS1 knockdown enhancing their myogenic differentiation, but reducing their self-renewal. Transfection with siRNA against PS1 led to accelerated myogenic differentiation during muscle regeneration in vivo. Conversely, constitutive expression of PS1 resulted in the suppression of myogenic differentiation and promotion of the self-renewal phenotype. Importantly, we found that PS1 also acts independently of its role in γ-secretase activity in controlling myogenesis, which is mediated in part by Id1 (inhibitor of DNA binding 1), a negative regulator of the myogenic regulatory factor MyoD. PS1 can control Id1, which affects satellite cell fate by regulating the transcriptional activity of MyoD. Taken together, our observations show that PS1 is a key player in the choice of satellite cell fate, acting through both γ-secretase-dependent and γ-secretase-independent mechanisms.

Key words: Satellite cell, Myoblast, Presenilin-1, Id1, Pax7, MyoD, γ-secretase, Self-renewal, Skeletal muscle, Myogenic differentiation, Stem cell, Cell fate choice

Introduction

Muscle satellite cells are myogenic stem cells that are located between the basal lamina and the plasmalemma of myofibers (Mauro, 1961). They are necessary for postnatal muscle growth, and are responsible for maintenance, hypertrophy and repair of adult skeletal muscle. It has been shown that satellite cells are able to self-renew to maintain their population (Collins et al., 2005) and much work is currently directed at understanding how self-renewal is regulated (reviewed by Zammit, 2008).

The paired-box transcription factor Pax7 is expressed by quiescent satellite cells and is implicated in the generation of committed myogenic progenitors, but its role in the regulation of satellite cell self-renewal is in debate (Lepper et al., 2009; McKinnell et al., 2008; Olguin et al., 2007; Seale et al., 2000; Zammit et al., 2006). Following activation, satellite cells co-express Pax7 with MyoD [a member of the myogenic regulatory factor family, together with Myf5, Mrf4 and Myog (myogenin)] and proliferate. Later, satellite-cell-derived myoblasts either downregulate Pax7, maintain MyoD and induce Myog as they undergo myogenic differentiation, or they downregulate MyoD and maintain Pax7, returning to a quiescent-like state (Halevy et al., 2004; Zammit et al., 2004). Interestingly, the total number of satellite cells in adult muscles remains relatively constant after repeated muscle injury and regeneration, indicating that the self-renewal system of satellite cells is carefully coordinated (Collins et al., 2005; Yoshida et al., 1998; Zammit et al., 2004). However, the molecular mechanism of satellite cell self-renewal remains poorly understood, although recent advances have shown that Notch and canonical Wnt signalling play a role (Brack et al., 2008; Conboy and Rando, 2002; Kitzmann et al., 2006; Kuang et al., 2007; Perez-Ruiz et al., 2008).

Notch signalling controls many events, including differentiation, proliferation and apoptosis in various tissues (Hansson et al., 2004). In skeletal muscle, the Notch-signalling pathway is involved in activation, and proliferation of muscle satellite cells, and has been implicated in their self-renewal (Conboy et al., 2003; Conboy and Rando, 2002; Kitzmann et al., 2006; Kopan et al., 1994; Kuang et al., 2007; Nofziger et al., 1999; Ono et al., 2007). For example, inhibition of Notch activity enhances myogenic differentiation of murine and human myoblasts (Kitzmann et al., 2006; Kuang et al., 2007). Notch is activated by binding of members of the delta-like and Jagged families (in mammals) to its extracellular domain, which results in γ-secretase-mediated cleavage to release the Notch intracellular domain (Notch ICD) (Herreman et al., 2000; Struhl and Greenwald, 1999; Zhang et al., 2000). The Notch ICD translocates into the nucleus, where it interacts with the DNA-binding protein CSL/RBP-J (RBP-J is a member of CSL family of proteins) to regulate the transcription of target genes such as *Hes1* (Jarriault et al., 1995).

Together with nicastrin, Pen-2 and Aph-1, the other crucial component of the γ-secretase complex is presenilin (reviewed by De Strooper, 2003). Presenilin-1 (PS1) and presenilin-2 (PS2) are membrane proteins that function as the catalytic subunit of the γ-secretase complex, an intramembrane protease with a number of substrates of the type I membrane protein family (De Strooper et al., 1999) (reviewed by Parks and Curtis, 2007; Vetrivel et al., 2006). For example, in addition to cleavage of activated Notch, γ-secretase targets also include, but are not limited to, amyloid precursor protein

(APP), Delta, Jagged, CD44, CD43, Erb4, E-cadherin, N-cadherin and syndecan (De Strooper et al., 1999) (reviewed by Parks and Curtis, 2007; Vetrivel et al., 2006). Importantly, PS1 also functions via γ-secretase-independent pathways (Akbari et al., 2004; Esselens et al., 2004; Huppert et al., 2005; Meredith et al., 2002; Repetto et al., 2007; Tu et al., 2006; Wilson et al., 2004). For example, somitogenesis is abrogated in *PS1*-null mice, yet embryos lacking other essential components of the γ-secretase complex, such as nicastrin, Pen-2 and Aph-1, or null for the Notch pathway component CSL/RBP-J, still develop anterior somites in the complete absence of Notch signalling (Huppert et al., 2005). Furthermore, the roles of PS1 in Ca^{2+} homeostasis (Akbari et al., 2004; Tu et al., 2006); autophagy and protein degradation (Esselens et al., 2004; Repetto et al., 2007; Wilson et al., 2004); and Wnt–β-catenin signalling (Meredith et al., 2002) have all also been shown to be via γ-secretase-independent mechanisms.

Here, we sought to explore the role of PS1 in satellite cell function. We found that PS1 is strongly expressed in activated and proliferating satellite cells, where PS1 knockdown accelerates myogenic differentiation and reduces the number of cells undergoing self-renewal. By contrast, constitutive PS1 expression led to a downregulation of MyoD expression and decreased differentiation. PS1 acts via Id1 (inhibitor of DNA binding 1), a potent negative regulator of the ability of MyoD to activate its transcriptional targets. Because *PS1*-null mice die during embryogenesis, we used *PS1*$^{-/-}$ and/or *PS2*$^{-/-}$ murine embryonic fibroblasts (MEFs) and found that Id1 levels were low, but significantly upregulated by addition of PS1 or a mutant PS1 that lacks γ-secretase activity, but not by PS2. Taken together, these observations show that PS1 has an essential role in satellite cell function, and can act independently of γ-secretase activity by regulating Id proteins to control MyoD transcriptional activity.

Results

PS1 is induced during activation of satellite cells

To investigate the expression dynamics of PS1 during myogenic progression, immunostaining was performed on satellite cells retained in their niche on isolated myofibres. PS1 was not detectable in Pax7$^+$ quiescent satellite cells, analysed immediately after isolation (T0). However, culture of myofibres in plating medium for 24 hours (T24) showed that activated satellite cells induced robust PS1 expression, located in the membrane compartment (Fig. 1A,E), which remained high in proliferating Ki67$^+$ or undifferentiated Pax7$^+$ satellite cells at T48 (Fig. 1A,B). PS1 was then downregulated in satellite cell progeny committed to myogenic differentiation after 72 hours (T72), as shown by the presence of Myog (Fig. 1C). PS1 was clearly expressed in Ki67$^+$ proliferating plated satellite-cell-derived myoblasts, but not in differentiating Myog$^+$ cells, 5 days after isolation (Fig. 1D). Using western blotting, we also confirmed that PS1 is highly expressed in plated proliferating satellite-cell-derived myoblasts, and decreased in cells induced to differentiate by switching to low-serum medium (Fig. 1F).

PS1 knockdown inhibits satellite cell self-renewal

Having shown that PS1 is expressed in activated and proliferating satellite cells, we next examined its function. In order to determine the effect of knockdown of PS1 on lineage progression in satellite-cell-derived myoblasts, cells were transfected with either of two siRNA duplexes against PS1 (PS1si-1 or PS1si-2) and control siRNA. Both siRNA species targeting PS1 effectively reduced PS1 protein levels in plated satellite-cell-derived myoblasts, when assayed 48 hours after transfection using western blot (Fig. 2A). At 72 hours after transfection, reduced PS1 levels resulted in a marked promotion of differentiation, as indicated by the higher fusion index for cells transfected with *PS1* siRNA than for cells

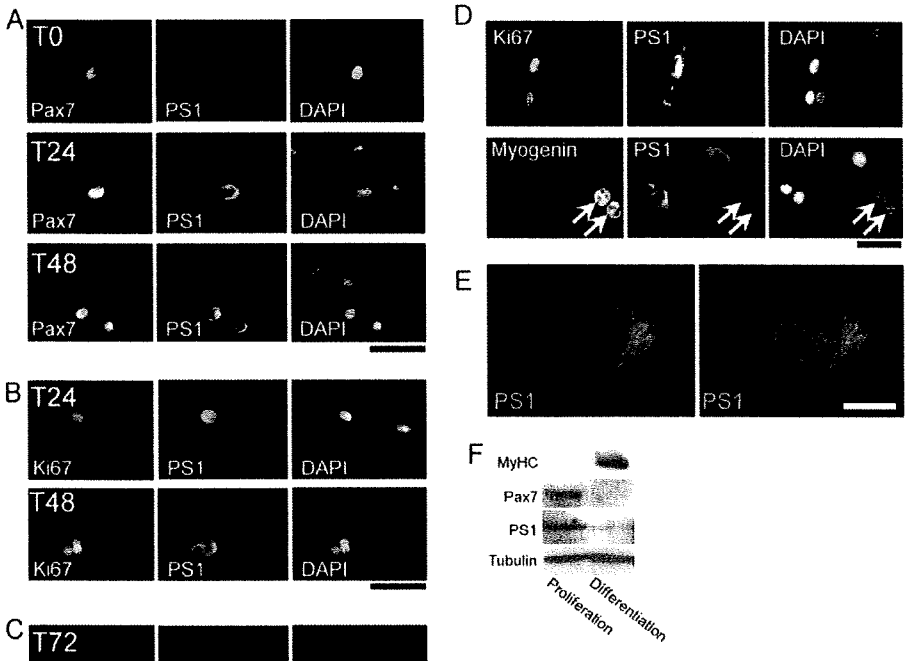

Fig. 1. PS1 is expressed by activated and proliferating satellite cells. Myofibres and their associated satellite cells were isolated and either immediately fixed (T0) or cultured in activation medium for either 24 hours (T24), 48 hours (T48) or 72 hours (T72) before fixation. (A) Immunostaining showed that Pax7$^+$ satellite cells on freshly isolated myofibres (T0) did not express PS1. (B) PS1 could be detected after activation and during proliferation, as shown by the co-expression of PS1 and Ki67. (C) PS1 was downregulated as satellite-cell-derived myoblasts committed to myogenic differentiation, as demonstrated by the presence of Myog (arrows). (D) Immunocytochemistry on plated satellite-cell-derived myoblasts confirmed that expression of PS1 was associated with proliferating Ki67$^+$ cells but not differentiating Myog$^+$ cells (arrows). (E) High magnification immunofluorecent image to show the localisation of PS1 in plated satellite-cell-derived cells. (F) Western blot to illustrate that PS1 expression decreases after myogenic differentiation in plated satellite-cell-derived cells. Representative data of at least three independent experiments are shown. Scale bars: 60 μm (A-C), 30 μm (D) and 5 μm (E).

transfected with control siRNA (fold change in the number of DAPI-stained nuclei of differentiated cells [as shown by the presence of myosin heavy chain (MyHC)] divided by the total number of DAPI-stained nuclei; Fig. 2B and quantified in 2C). Importantly, siRNA-mediated knockdown of PS1 drastically reduced both the number of $Pax7^+$ cells and the percentage of cells with the $Pax7^+MyoD^-$ self-renewal phenotype (Zammit et al., 2004), compared with controls (Fig. 2D and quantified in 2E,F).

Transfection of *PS1* siRNA was also performed to assay the effects of PS1 knockdown on the fate of satellite cells retained in their niche on the myofibre. First, we determined the transfection efficiency of siRNA into satellite cells on a myofibre by using AlexaFluor488-conjugated siRNA (Fig. 2G) and found that levels of >95% could be obtained, and that PS1 was successfully knocked down (Fig. 2G). The percentage of $Pax7^+MyoD^-$ self-renewed cells was significantly decreased 72 hours after transfection with *PS1* siRNA, with an increased amount of differentiation-committed $Pax7^-MyoD^+$ and $Pax7^-Myog^+$ cells present, in comparison with cells transfected with control siRNA (Fig. 2H and quantified in 2I,J). Thus, PS1 is required for satellite cell self-renewal and for inhibition of myogenic differentiation.

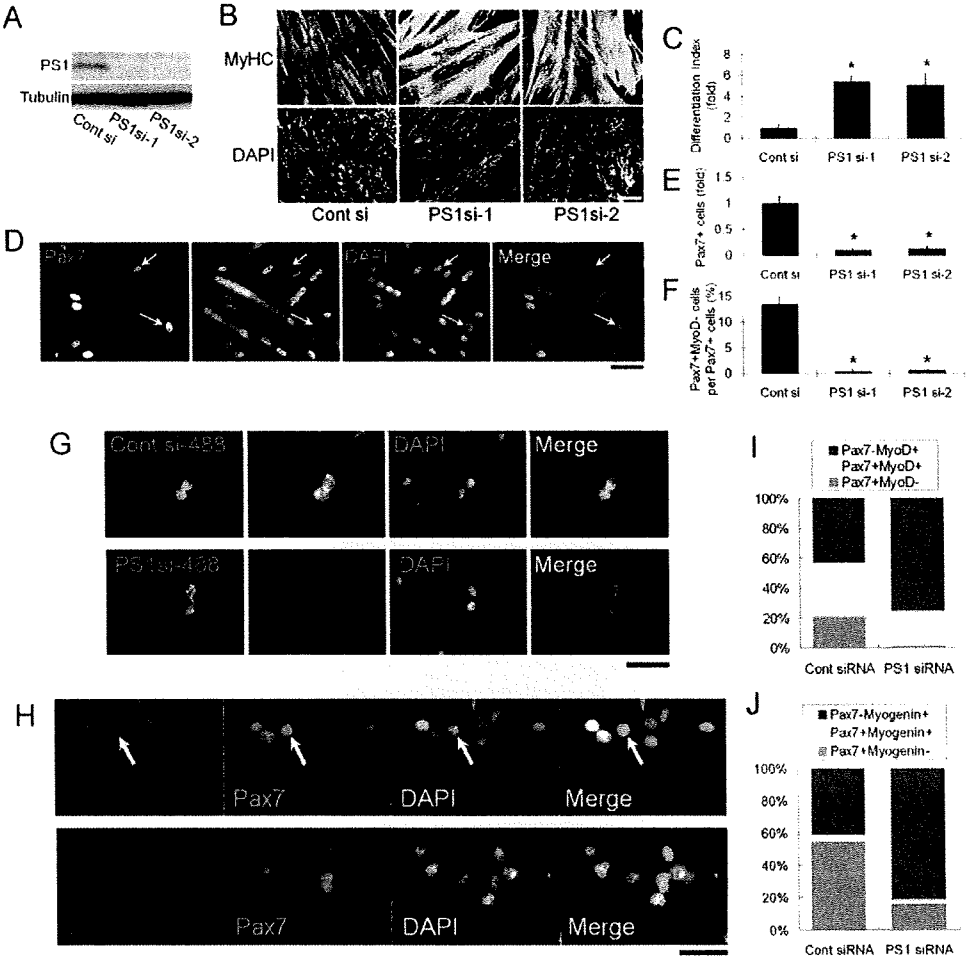

Fig. 2. PS1 is required for satellite cell self-renewal and maintenance of progenitor cells. To examine the effects of PS1 on satellite cell myogenic progression, we first knocked-down PS1 protein levels using siRNA. (A) Both *PS1* siRNAs (PS1si-1 and PS1si-2) efficiently knockdown PS1 protein in plated primary satellite-cell-derived myoblasts as shown by western blotting. (B) Satellite-cell-derived myoblasts were cultured for 3 days after siRNA transfection and then immunostained for MyHC. A dramatic increase in the extent of myogenic differentiation and formation of myotubes was observed with both siRNA species directed against PS1 as compared to controls (Cont si). (C) Differentiation index quantifying the increased myogenic differentiation caused by PS1 knockdown, calculated as fold change in the number of DAPI-stained nuclei in $MyHC^+$ cells, divided by the total number of DAPI-stained nuclei. (D) Immunocytochemistry of plated primary myoblasts was also used to investigate the presence of cells with a self-renewal phenotype ($Pax7^+MyoD^-$) 3 days after siRNA transfection (arrows indicate $Pax7^+MyoD^-$ cells), and clearly demonstrate that reduced PS1 levels resulted in less $Pax7^+$ cells (quantified in E) and self-renewal (quantified in F). (G) AlexaFluor488-conjugated control siRNA and *PS1* siRNA duplexes were transfected into satellite cells retained in their niche on isolated myofibres, and knockdown of PS1 protein confirmed by immunocytochemistry 48 hours later. (H) The effects of PS1 knockdown on satellite cell fate were examined by immunostaining for Pax7, MyoD (arrows indicates $Pax7^+MyoD^-$ cell) and Myog 72 hours after PS1si-1 transfection. (I,J) PS1 knockdown reduced the percentage of satellite-cell-derived myoblasts exhibiting the self-renewal phenotype ($Pax7^+MyoD^-$), while increasing the percentage of cells committed to differentiation ($Pax7^-MyoD^+$ and $Pax7^-Myog^+$). Data from at least three independent experiments is shown ± s.d. Asterisks in C, E and F indicate that data are significantly different from control values ($P<0.05$). Scale bars: 100 μm (B), 30 μm (D,G,H).

Constitutive PS1 expression inhibits myogenic differentiation

Notch is activated by the binding of its ligands, and activated Notch is then cleaved by γ-secretase to release the Notch ICD, a central step in Notch signalling. Although γ-secretase activity is dependent on PS1 function, several studies have reported that overexpression of PS1 alone does not enhance γ-secretase activity, unless in conjunction with nicastrin, Aph-1a and Pen-2 (reviewed by De Strooper, 2003; Parks and Curtis, 2007; Vetrivel et al., 2006). To investigate the effect of constitutive PS1 expression on satellite cell function, mouse *PS1* cDNA was cloned to generate *pMSCV-PS1-IRES-GFP* or *pCMV-PS1-V5*. *pMSCV-PS1-IRES-GFP* was transfected into satellite-cell-derived myoblasts, with eGFP from the *IRES-eGFP* allowing transfected cells to be readily identified (transfection efficiency was >30% for both vectors). Constitutive PS1 expression led to fewer $eGFP^+$ cells containing MyHC (8%) (Fig. 3A and quantified in 3D) or $MyoD^+$ (62%) (Fig. 3B and quantified in 3E) compared with cells transfected with control empty *pMSCV-IRES-GFP*. Constitutive expression of PS1 also significantly increased the number of $eGFP^+$ cells expressing Pax7 by approximately fourfold over parallel cultures transfected with control siRNA (Fig. 3C and quantified in 3F).

To confirm that transfection of PS1 does not act by increasing γ-secretase activity, constitutive PS1 expression was also examined in the presence of DAPT, which is a specific pharmacological inhibitor of γ-secretase activity (Lammich et al., 2002). Importantly, the effects of PS1 on increasing the number of $eGFP^+$ satellite-cell-derived myoblasts containing Pax7 protein, was not significantly altered when γ-secretase activity was inhibited (Fig. 3F). Because inhibition of γ-secretase normally results in a decrease in Pax7 expression, these observations indicate that PS1 is exerting its effect through a mechanism that is independent of γ-secretase activity. Taken together, these results clearly demonstrate that myogenic differentiation was suppressed by overexpression of PS1, but the number of cells expressing Pax7 significantly rose, via a mechanism independent of γ-secretase activity.

PS1 negatively regulates expression of MyoD through a γ-secretase-independent mechanism

To perform detailed biochemical analysis, we also used the immortalised adult post-injury-derived C2 cell line (Yaffe and Saxel, 1977). Immunocytochemistry showed that PS1 was expressed in proliferating C2C12 myoblasts (data not shown), as observed in primary satellite-cell-derived myoblasts (Fig. 1). Both siRNAs targeting PS1 effectively reduced PS1 protein levels 48 hours after transfection in C2C12 cells (Fig. 4A) and enhanced myogenic differentiation after 72 hours in differentiation medium (DM), with

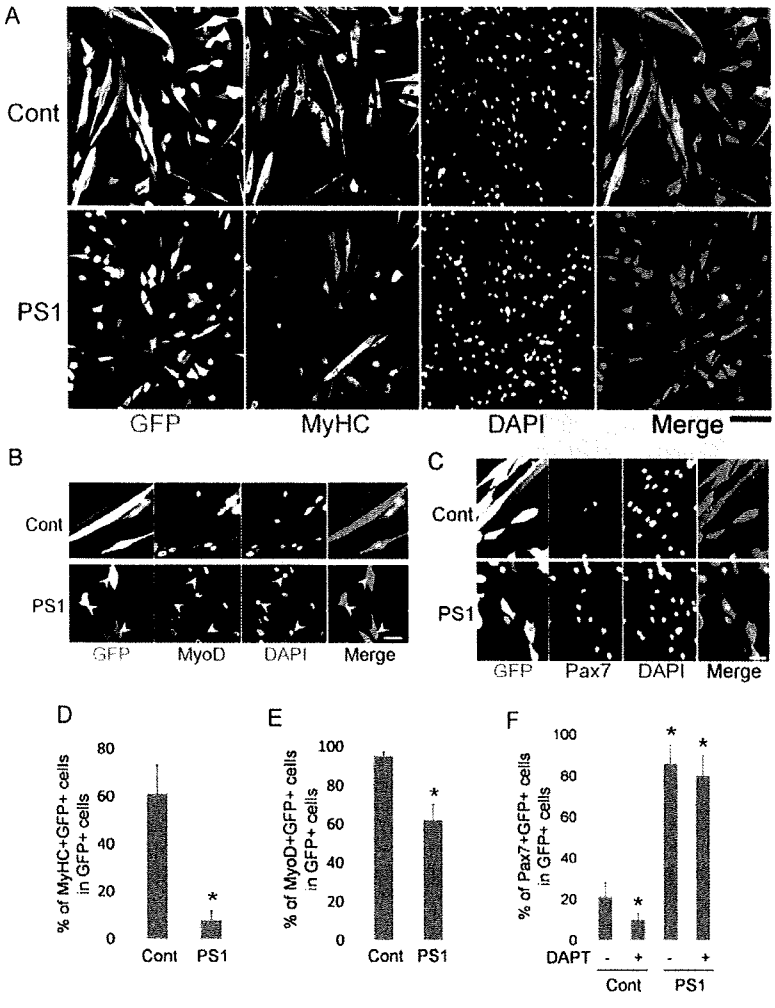

Fig. 3. Constitutive PS1 expression leads to suppression of myogenic differentiation and augmentation of Pax7 expression. The effects of PS1 on satellite cell function were examined by constitutively expressing PS1 using expression vectors. (A,B) Primary satellite-cell-derived myoblasts were transfected with either control *pMSCV-IRES-GFP* (Cont) or *pMSCV-PS1-IRES-GFP* (PS1) vectors and, 48 hours later, immunostained for eGFP (to identify transfected cells) and either MyHC (A) or MyoD (B) (arrowheads indicate GFP^+MyoD^- cells in PS1-vector-transfected cells). (D,E) Constitutive PS1 expression significantly reduced the percentage of transfected cells that co-expressed either MyHC (D), or MyoD (E). (C,F) Constitutive PS1 expression also increased the percentage of satellite-cell-derived myoblasts expressing Pax7. (F) Although exposure of control *pMSCV-IRES-GFP*-transfected cells to 1 μM DAPT reduced the percentage of Pax7-expressing cells, DAPT inhibition of γ-secretase did not prevent the significant increase of Pax7 in transfected cells containing *pMSCV-PS1-IRES-GFP* vector. Data from at least three independent experiments is shown ± s.d. Asterisks in D-F indicate that data are significantly different from control values ($P<0.05$). Scale bars: 100 μm (A) and 30 μm (B,C).

larger multinucleated myotubes formed than in control cultures (Fig. 4B). Even when maintained in growth medium (GM), transfection with either of the *PS1* siRNA species resulted in an induction of MyHC expression (Fig. 4B), though crucially, treatment with DAPT alone, to inhibit γ-secretase activity, did not result in MyHC expression (Fig. 4B). Immunblot analysis of C2C12 cells transfected with *PS1* siRNAs also revealed a lower expression of Pax7 with both duplexes than with control siRNA (Fig. 4D).

Transfection of *pMSCV-PS1-IRES-GFP* into C2C12 myoblasts resulted in high levels of PS1 and GFP protein in >70% of cells (Fig. 4E), allowing us to perform western blot analysis. As with primary satellite-cell-derived myoblasts, transfection with *pMSCV-PS1-IRES-GFP* resulted in a marked suppression of MyHC expression compared with control (Fig. 4F). Again, constitutive PS1 expression-mediated inhibition of differentiation was not influenced by the presence of DAPT to inhibit γ-secretase activity (Fig. 4G and quantified in 4H). Importantly, immunoblot analysis for Notch1 ICD, Notch2 ICD and Hes1 showed that the already-active Notch signalling in proliferating myoblasts was not further augmented by constitutive PS1 expression (Fig. 4I). Interestingly, expression of MyoD was downregulated by constitutive expression of PS1 in proliferating myoblasts, but expression of Pax7 was not affected (Fig. 4I). To check whether MyoD downregulation was influenced by γ-secretase activity, we transfected C2C12 myoblasts with *pCMV-V5-tagged PS1* in the presence of DAPT to inhibit γ-secretase activity, and found that MyoD levels still decreased significantly (Fig. 4J and quantified in 4K).

Myogenic differentiation in *PS1*-null cells is independent of γ-secretase activity

Mice homozygous for null alleles of *PS1* die late in embryogenesis (Shen et al., 1997; Wong et al., 1997), precluding examination of satellite cells. To model myogenesis in *PS1*-null cells therefore, we used ectopic MyoD expression to initiate myogenic conversion in MEFs (Skapek et al., 1996). Immunostaining revealed robust expression of PS1 in control wild-type (WT) MEFs but not *PS1*$^{-/-}$

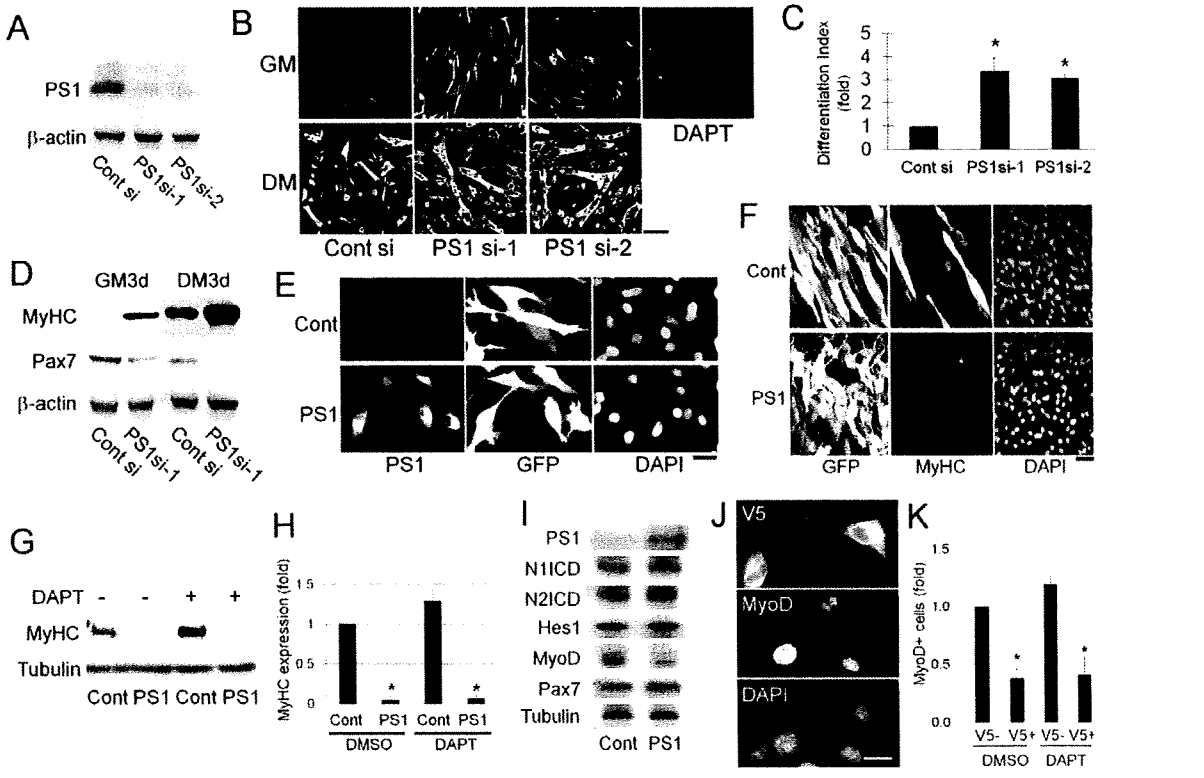

Fig. 4. PS1 negatively regulates MyoD expression in a γ-secretase-independent mechanism. In order to obtain sufficient material for biochemical analysis, we also used the adult mouse muscle-derived C2C12 myogenic cell line. (A) Immunoblot analysis showed that proliferating C2C12 cells expressed PS1, and that the siRNA-targeting PS1 (PS1si-1 and PS1si-2) was effective at reducing PS1 protein levels. (B) As with primary myoblasts, exposure of C2C12 myoblasts to siRNA against PS1 promoted myogenic differentiation, as shown by immunostaining for MyHC, in both growth (GM) and differentiation medium (DM) (quantified in C for DM). Importantly, treatment with DAPT in GM for 3 days to inhibit γ-secretase activity did not reproduce the effects of PS1 knockdown, being unable to induce expression of MyHC in C2C12 cells. (D) Immunblot analysis of siRNA-transfected C2C12 cells cultured in GM or DM for 3 days after transfection confirmed increased MyHC expression. Importantly, Pax7 levels were significantly reduced by PS1 knockdown under both culture conditions. (E-I) PS1 was also constitutively expressed in C2C12 myoblasts by transient transfection with PS1-expression vector (*pMSCV-PS1-IRES-GFP*). (F) Immunocytochemical analysis for MyHC revealed that myogenic differentiation was again inhibited. (G) Immunoblot analysis of transfected C2C12 cells constitutively expressing PS1, illustrating that inhibiting γ-secretase activity by exposure to 1 μM DAPT for 2.5 days did not alter the marked reduction in MyHC levels (quantified in H). (I) Immunoblot analysis demonstrated that constitutive PS1 expression in C2C12 cells cultured in GM for 24 hours after transfection did not affect the levels of Notch1 ICD, Notch2 ICD or Hes1, but that MyoD was significantly reduced, compared to the tubulin protein loading control. (J) Similar results were obtained using a V5-tagged PS1 expression vector transfected into C2C12 cells. Immunostaining showed that MyoD expression was reduced to a similar degree, with or without exposure to 1 μM DAPT to inhibit γ-secretase activity (quantified in K). Data from at least three independent experiments is shown ± s.d. Asterisks in C, H and K indicate that data are significantly different from control values (P<0.05). Scale bars: 100 μm (B), 20 μm (E), 30 μm (F) and 10 μm (J).

MEFs (Fig. 5A). γ-secretase activity was significant lower in *PS1*$^{-/-}$ MEFs than in control WT MEFs, as assessed using a γ-secretase activity detection kit (data not shown).

Transient transfection with a MyoD expression vector resulted in robust MyoD expression in both WT and *PS1*$^{-/-}$ MEFs (Fig. 5B). Myogenic differentiation in vitro is suppressed by culture in medium containing high levels of serum (Kodaira et al., 2006), and we observed no signs of myogenic differentiation in WT MEFs maintained in 10% FBS for 5 days after transfection with MyoD (Fig. 5C,D). By contrast, robust MyHC expression and formation of multinucleated myotubes occurred in MyoD-transfected *PS1*$^{-/-}$ MEFs maintained under identical high-serum conditions (Fig. 5C,D). Under low-serum (2% FBS) conditions, MyoD-transfected *PS1*$^{-/-}$ MEFs also had higher MyHC levels than control-transfected WT MEFs (data not shown). We next investigated whether this MyoD-induced myogenesis in *PS1*$^{-/-}$ MEFs could be 'rescued' by PS1. Transfection with PS1 expression vectors completely inhibited the MyoD-induced myogenic differentiation of *PS1*$^{-/-}$ MEFs (Fig. 7K).

To determine whether this process is independent of γ-secretase activity, we used the γ-secretase inhibitors DAPT and L-685,458 on MyoD-transfected *PS1*$^{-/-}$ MEFs and WT MEFs. γ-secretase activity was significantly decreased in WT MEFs (~93%) after 1 μM DAPT treatment, as determined using a γ-secretase activity detection kit (data not shown). We found that neither treatment with DAPT (even up to 50 μM; data not shown) nor L-685,458 could induce myogenic differentiation in MyoD-expressing WT MEFs in high-serum medium, or changed high MyHC expression levels in MyoD-containing *PS1*$^{-/-}$ MEFs (Fig. 5E and quantified in 5F). Together, these observations suggest that the MyoD-induced myogenic program is inhibited by PS1 in a manner that is independent of γ-secretase activity.

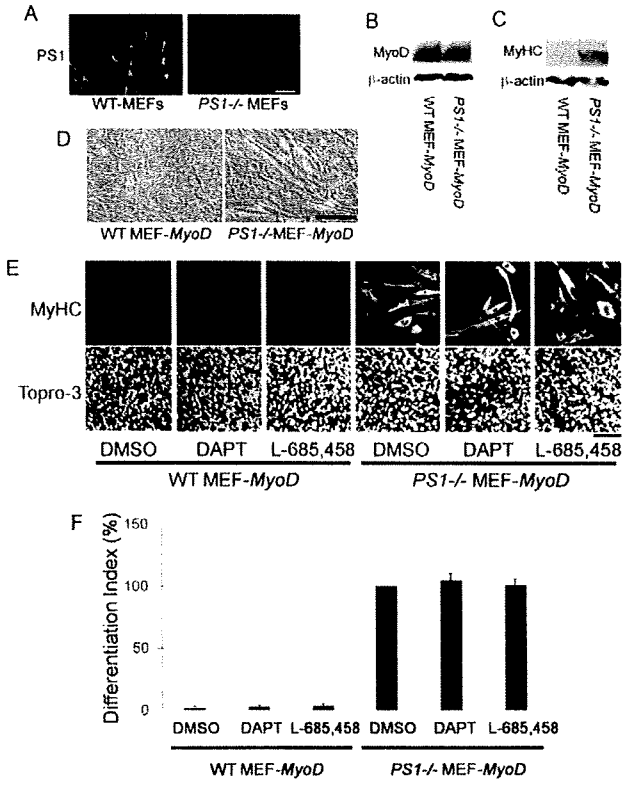

Fig. 5. Induced myogenic differentiation of *PS1*$^{-/-}$ MEFs is independent of γ-secretase activity. *PS1*$^{-/-}$ mice die during embryogenesis and so, to examine myogenesis, we used MyoD-transfected MEFs. (A) Immunostaining revealed that PS1 is expressed by WT MEFs, but is absent from *PS1*$^{-/-}$ MEFs. (B,C) Immunoblot analysis demonstrated that myogenesis was effectively induced in *PS1*$^{-/-}$ MEFs by transfection of a MyoD-expression vector. β-actin was the protein loading control. (C,D) Culture in high-serum (10% FBS) medium for 5 days still resulted in MyHC expression (C) and formation of myotubes (D) in *PS1*$^{-/-}$ MEFs, but not in WT. (E,F) WT MEFs transfected with the MyoD-expression-vector and exposed to 1 μM DAPT or 1 μM L-685,458 to inhibit γ-secretase activity failed to induce MyHC expression when cultured in 10% FBS for 5 days. However, MyoD-transfected *PS1*$^{-/-}$ MEFs, maintained under identical culture conditions, differentiated and expressed MyHC, with inhibition of γ-secretase activity having no effect on the differentiation index. Data from at least three independent experiments are shown ± s.d. Scale bars: 20 μm (A), 100 μm (D) and 60 μm (E).

PS1 regulates Id1 expression in myogenic cells

Despite the high-serum culture conditions, our results show that myogenic differentiation is clearly induced by ectopic MyoD expression in *PS1*$^{-/-}$ MEFs (Fig. 5). BMP (bone morphogenetic protein) signalling contributes to serum-induced inhibition of myogenic differentiation in vitro (Kodaira et al., 2006) and *Id1* is a major BMP signalling downstream target gene, known to be a potent negative regulator of MyoD in myoblasts (Benezra et al., 1990; Jen et al., 1992; Katagiri et al., 2002). We hypothesised therefore, that Id1 might also be regulated by PS1. To test this, immunostaining was performed to investigate whether satellite cells express Id1 during myogenic progression. Id1 was not detectable in Pax7^{+} quiescent satellite cells (T0), but was upregulated in activated and proliferating satellite cells (T72; Fig. 6A). Id1 was then downregulated in myoblasts committing to myogenic differentiation, as shown by the presence of Myog or absence of Pax7 (arrow; Fig. 6A,B), showing that the Id1 expression profile mirrors that of PS1 (Fig. 1).

To determine whether the levels of PS1 and Id1 were causally linked in myoblasts, we transfected satellite-cell-derived myoblasts with *pMSCV-PS1-IRES-GFP* and found high Id1 levels in eGFP^{+} (PS1-expressing) cells (Fig. 6C). Constitutive PS1 expression in C2C12 cells also resulted in upregulation of the level of Id1 protein on immunoblots (Fig. 6D and quantified in 6E). Consistent with the observations that PS1 promotes Id1, knockdown of PS1 levels using siRNA in C2C12 myoblasts, led to a dramatic decrease in Id1 expression levels (Fig. 6F). Constitutive PS1 expression did not influence Pax7 protein levels (Fig. 4I), and in accord with this, increased Id1, did not change Pax7 expression in C2C12 myoblasts transfected with *pCMV-Id1* (Fig. 6G).

PS1 regulates Id1 expression with a γ-secretase independent mechanism

Constitutive PS1 expression still caused an increase in Id1 in C2C12, even when γ-secretase activity was inhibited using DAPT (Fig. 6D,E). This response was not restricted to myogenic cells, however: in the mesenchymal stem cell line 10T1/2, constitutive PS1 expression again increased Id1 protein levels, independently of γ-secretase activity (Fig. 7A). To further examine PS1 regulation of Id1, we performed immunocytochemical analysis to assay Id1 protein in *PS1*$^{-/-}$ MEFs, and found that Id1 expression was lower in *PS1*$^{-/-}$ MEFs than in WT MEFs. This was again independent of γ-secretase activity because inhibition with DAPT did not influence Id1 expression in WT MEFs (Fig. 7B). This decreased level of Id1

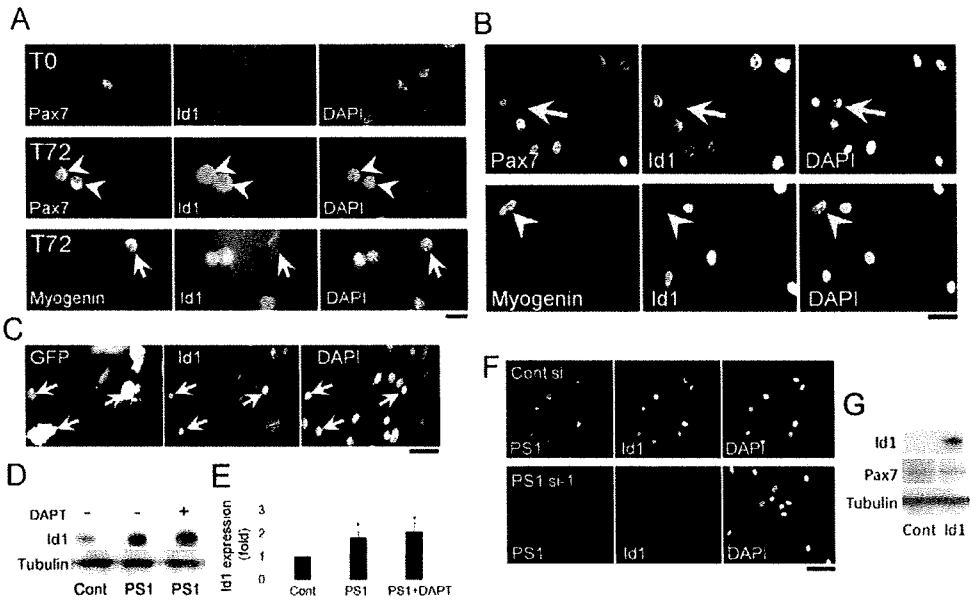

Fig. 6. PS1 regulates the expression of Id1, to function independently of Notch signalling. (A) Immunocytochemical analysis for Pax7 and Id1 on satellite cells associated with a myofibre demonstrated that Id1 was not present in quiescent satellite cells (T0). By 72 hours (T72) after isolation, Id1 was robustly expressed in Pax7-expressing cells (arrowheads), but downregulated in satellite-cell-derived myoblasts as they commit to myogenic differentiation (arrows), as shown by co-immunostaining for Id1 and Myog. (B) In plated satellite-cell-derived myoblasts, again Id1 expression was associated with undifferentiated cells (arrows, $Pax7^-$ cells; arrowheads, $Myog^+$ cells). (C) Constitutive expression of PS1 by transfection of satellite-cell-derived myoblasts with *pMSCV-PS1-IRES-eGFP* resulted in eGFP (PS1)-containing cells also having robust Id1 expression, revealed by immunostaining (arrows, GFP^+Id1^+ cells). (D) Immunoblotting of C2C12 myoblasts transfected with a PS1-expression vector (PS1) showed that Id1 levels were significantly increased. This PS1-induced increase in Id1 levels was not affected by exposure to 1 μM DAPT for 6 hours to inhibit γ-secretase activity (quantified in E). (F) The effect of *PS1* siRNA on expression of Id1 in satellite-cell-derived myoblasts was analysed by immunostaining, and demonstrated that PS1 and Id1 were colocalised in cells transfected with control siRNA (Cont), but revealed that siRNA-mediated knockdown of PS1 resulted in less Id1 expression. (G) Immunoblotting analysis showed that constitutive Id1 expression did not change Pax7 expression levels in C2C12 myoblasts transfected with the *pCMV-Id1* expression vector. Data from at least three independent experiments are shown ± s.d. Asterisks in E indicate that data are significantly different from control values ($P<0.05$). Scale bars: 10 μm (A), 20 μm (B), 30 μm (C) and 50 μm (F).

protein in $PS1^{-/-}$ MEFs was also confirmed by immunoblotting (Fig. 7C). Because MyoD-induced myogenesis in $PS1^{-/-}$ MEFs could be 'rescued' by PS1 (Fig. 7K), we also transfeced $PS1^{-/-}$ MEFs with the Id1 expression vector, *pCMV-Id1*, and again found a complete inhibition of MyoD-induced myogenic differentiation in high-serum medium (Fig. 7K).

To separately confirm that PS1 regulates Id1 in a γ-secretase-activity-independent manner, we used a mutant *PS1* (*D385C PS1*) that encodes a PS1 protein with an Asp385 mutation that completely abolishes γ-secretase activity but still allows complex formation (Tolia et al., 2006). $PS1^{-/-}PS2^{-/-}$ MEFs stably expressing *D385C PS1* and another line carrying a control PS1 (*Cys-less PS1*) with full γ-secretase activity, both produced protein, as shown by immunostaining with PS1 (N-terminal) antibody (Fig. 7D). As expected, *D385C PS1* was not recognised by an anti-PS1 (cleaved loop domain) antibody that detected the *Cys-less PS1* control (Fig. 7E) (Tolia et al., 2006). Crucially, Id1 protein was increased in both $PS1^{-/-}PS2^{-/-}$ MEFs expressing *D385C-PS1* and control $PS1^{-/-}PS2^{-/-}$ MEFs expressing *Cys-less PS1* (Fig. 7E-G), demonstrating again that γ-secretase activity is not required for PS1-mediated Id1 upregulation.

PS1, but not PS2, regulates Id1 expression

There is evidence that PS1 and PS2 might have partially overlapping functions (reviewed by Vetrivel et al., 2006). However, the reduced Id1 levels found in $PS1^{-/-}$ MEFs was not observed in $PS2^{-/-}$ MEFs, whose Id1 levels were comparable with WT MEFs (Fig. 7B). To specifically test the effects of PS2 on Id1 expression, we performed immunoblot analysis in C2C12 myoblasts transfected with *PS2* siRNA and found that the significantly reduced PS2 protein levels did not affect Id1 (Fig. 7H quantified in 7I,J), in contrast to the effects of *PS1* siRNA (Fig. 6F). Furthermore, $PS2^{-/-}$ MEFs are refractory to MyoD-induced myogenic differentiation in high-serum culture conditions, in contrast to $PS1^{-/-}$ MEFs, confirming that there are non-redundant functions between the PS1 and PS2 (Fig. 7K).

PS1 knockdown accelerates myogenic differentiation in regenerating skeletal muscle in vivo

Finally, we evaluated the significance of PS1 to regenerating muscle in vivo. Cardiotoxin was used to induce muscle damage in the gastrocnemius of adult C57BL/6N mice and 12 hours later, the muscle was directly injected with 50 μl of 10 μM siRNA in Atelocollagen, a potent siRNA delivery mediator in vivo (Kinouchi et al., 2008). Four different conditions were used: saline control, control siRNA, PS1 si-1 and PS1 si-2. Regenerating muscles were isolated 3.5 days after cardiotoxin injection and frozen in liquid nitrogen before being cryosectioned. Muscle regeneration was assayed by immunostaining muscle sections for developmental MyHC (dMyHC), which is transiently expressed in regenerating myofibres, and phosphorylated histone H3 (p-histone H3) was used as a proliferation marker (Fig. 8). PS1 knockdown resulted in a significant induction of dMyHC expression (Fig. 8A and quantified

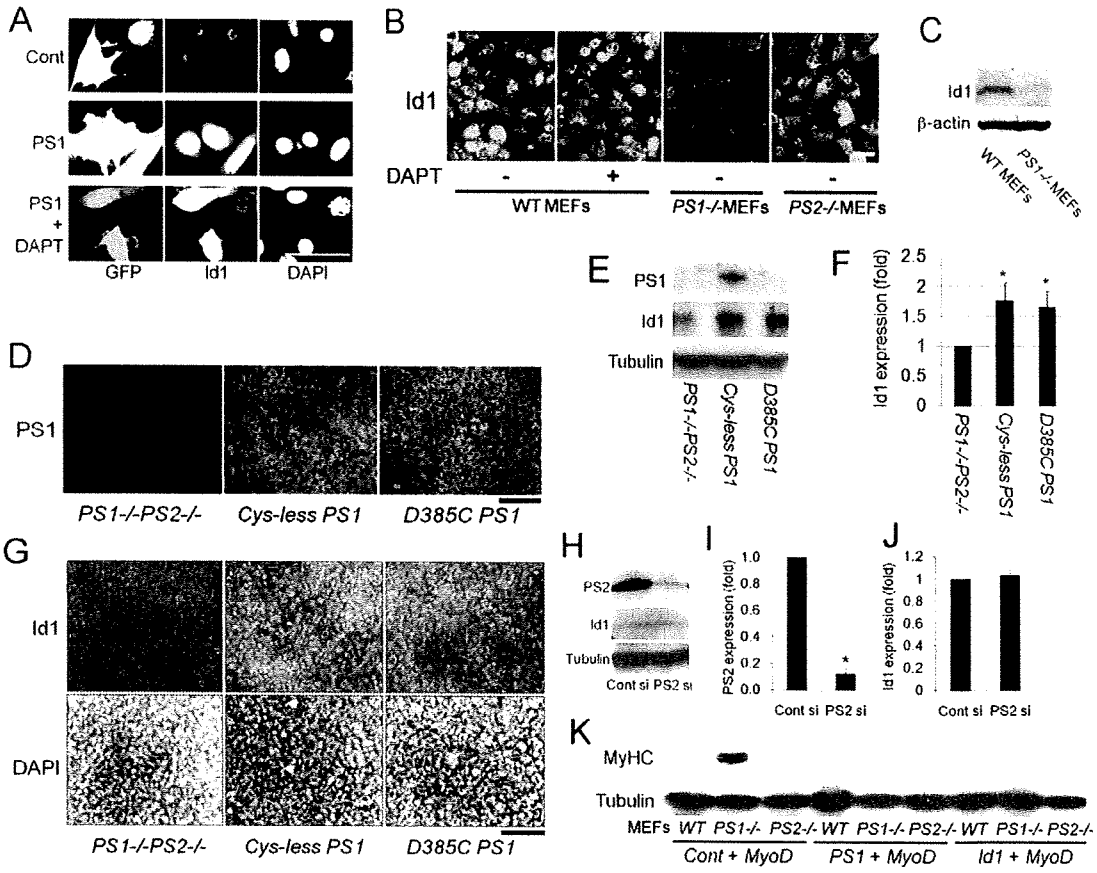

Fig. 7. PS1 controls Id1 expression in non-muscle cells via a γ-secretase-activity-independent mechanism. (A) PS1-regulated Id1 expression was not restricted to myogenic cells: in the mesenchymal stem cell line 10T1/2, immunostaining showed that constitutive PS1 expression increased Id1 protein levels, which was also independent of γ-secretase activity, as shown by exposure to 1 μM DAPT for 6 hours. (B) Immunostaining showed that reduction in Id1 levels was specific to *PS1*$^{-/-}$ MEFs because *PS2*$^{-/-}$ MEFs had robust Id1 levels, comparable to WT MEFs. Exposure of WT MEFs to 1 μM DAPT for 12 hours did not result in a reduction in Id1 levels. (C) Although Id1 was clearly present in WT MEFs, immunoblot analysis demonstrated that Id1 was expressed at very low levels from *PS1*$^{-/-}$ MEFs. β-actin was used as a control for protein loading. (D) Immunostaining showed that anti-PS1 (N-terminal) antibody recognised both stably inserted *D385C PS1* (PS1 mutant with no γ-secretase activity) and control *Cys-less PS1* in *PS1*$^{-/-}$*PS2*$^{-/-}$ MEFs. (E) Immunoblot analysis revealed that PS1 protein in *D385C-PS1*-inserted *PS1*$^{-/-}$*PS2*$^{-/-}$ MEFs was not detected by anti-PS1 (cleaved loop domain) antibody, which recognised the *Cys-less PS1*-inserted *PS1*$^{-/-}$*PS2*$^{-/-}$ MEFs. (E,F). Id1 protein was increased in both *Cys-less PS1* and *D385C-PS1* expressing *PS1*$^{-/-}$*PS2*$^{-/-}$ MEFs (quantified in F). (G) Immunostaining confirmed that *D385C PS1* inserted into *PS1*$^{-/-}$PS2$^{-/-}$ MEFs can upregulate Id1 protein, as does the control *Cys-less PS1*-inserted *PS1*$^{-/-}$*PS2*$^{-/-}$ MEFs. (H) Immunoblot analysis illustrates that specific siRNA-mediated knockdown of PS2 does not affect the level of Id1 protein in C2C12 myoblasts (quantified in I,J). (K) Immunoblotting 5 days after transfection illustrated that the presence of a MyoD-expression vector resulted in myogenic differentiation in *PS1*$^{-/-}$ MEFs maintained in high-serum culture conditions, as shown by the presence of MyHC. By contrast, WT or *PS2*$^{-/-}$ MEFs did not undergo myogenic conversion. Importantly, co-transfection of the MyoD expression vector with either a PS1-expression vector, or an Id1-expression vector, largely blocked this induction of MyHC in *PS1*$^{-/-}$ MEFs. Tubulin was used as an internal control for protein loading. Data from at least three independent experiments are shown ± s.d. Asterisks in F, I and J indicate whether data are significantly different from control values (P<0.05). Scale bars: 30 μm (A), 10 μm (B) and 100 μm (D,G).

in 8B) and a significant reduction in the number of cells containing p-histone H3 (Fig. 8C and quantified in 8D) compared with control siRNA. These observations indicate that PS1 is required for maintenance of proliferating cells and inhibition of myogenic differentiation during muscle regeneration in vivo as well as in vitro.

Discussion

Understanding how the decision between self-renewal and differentiation is regulated in satellite cells is central to understanding how skeletal muscle maintains a viable stem cell compartment. Here, we show that the multifunctional protein PS1 is able to direct muscle satellite cells away from myogenic differentiation and towards the self-renewal phenotype. Although PS1 is a key component of the γ-secretase complex, we found that PS1 also acts through γ-secretase-independent mechanisms to affect satellite cell fate, by controlling Id1 protein.

Satellite cells are normally mitotically quiescent in mature muscle, so must first be activated to enter the cell cycle and generate myoblasts (Zammit, 2008). Important pathways associated with activation include sphingolipid (Nagata et al., 2006b; Nagata et al., 2006a), p38MAPK (Jones et al., 2005) and Notch signalling (Conboy and Rando, 2002). Notch signalling in proliferating satellite cells plays a role in expanding the satellite cell pool after activation, while preventing precocious differentiation (Conboy et al., 2003; Conboy and Rando, 2002; Kitzmann et al., 2006; Kopan et al., 1994; Kuang et al., 2007; Nofziger et al., 1999). When PS1

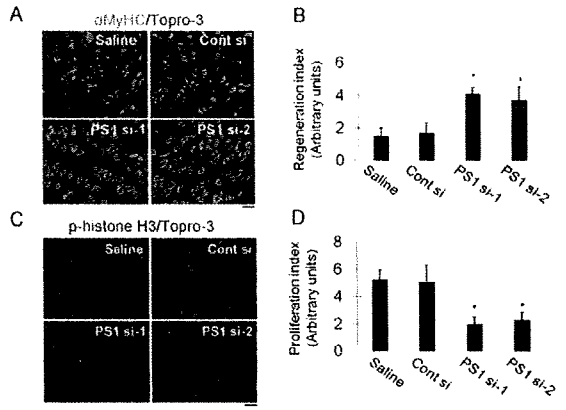

Fig. 8. PS1 maintains proliferation and inhibits precocious differentiation during muscle regeneration in vivo. Regeneration was induced in mouse gastrocnemius muscles by injection of cardiotoxin and, 12 hours later, injection of 50 µl of 10 µM siRNA in Atelocollagen. We employed four different conditions: saline control, control siRNA, PS1si-1 and PS1si-2. Then, 3.5 days after cardiotoxin injection, the muscles were removed, frozen and cryosectioned. (A,B) Muscle regeneration was assayed by immunostaining with Topro-3 for developmental MyHC (dMyHC), which is transiently expressed in regenerating muscle. PS1 knockdown resulted in a significant induction of dMyHC expression compared to controls (quantified in B). (C,D) Immunostaining for phosphorylated histone H3 (p-histone H3) was used as a proliferation marker. A significant reduction of p-histone $H3^+$ cells was observed in muscles exposed to siRNAs against PS1, compared with controls (quantified in D). The bar charts of regeneration index (B) or proliferation index (D) were calculated from the staining intensity of dMyHC-stained regenerating fibres (from A) or the number of p-histone H3-stained proliferating cells (from C), divided by the total number of nuclei in the field of randomly selected sections (n=5 for each condition). Values are means ± s.d. Asterisks in B and D indicate that data are significantly different from values obtained using control siRNA (P<0.05). Scale bars: 70 µm.

is knocked down using siRNA, we observe an increase in cells undergoing myogenic differentiation, with fewer expressing Pax7; a similar phenotype to that observed when Notch signalling is prevented by inhibiting γ-secretase activity using pharmacogical reagents such as DAPT and L-685,458 (Kitzmann et al., 2006; Kuang et al., 2007). Considering the crucial role of PS1 in the γ-secretase complex, PS1 knockdown will directly affect Notch signalling and so some effects on satellite cells are due to perturbation of this pathway. Importantly, not all effects of siRNA knockdown of PS1 in myoblasts could be reproduced by simply inhibiting γ-secretase activity. For example, PS1 knockdown in myoblasts maintained even under high serum conditions, resulted in a high degree of myogenic differentiation, an observation not repeated when only γ-secretase activity was inhibited (Fig. 4B). Therefore, PS1 is also operating independently of its role in the γ-secretase complex. We found that PS1 knockdown also reduces the level of Id1 protein in C2C12 myoblasts. Id1 has been shown to dimerise with basic helix-loop-helix transcription factors such as MyoD, and to inhibit their transcriptional activity (Benezra et al., 1990; Jen et al., 1992). Therefore, reduced Id1 levels would alleviate a block on MyoD transcriptional activity and so lead to induction of Myog and myogenic differentiation. Myog has been shown to indirectly inhibit Pax7 expression (Olguin et al., 2007), thus providing a mechanism by which differentiation and self-renewal are linked through MyoD transcriptional activity. Furthermore, it has been reported that inhibition of myogenic differentiation by forced expression of Notch ICD is not accompanied by *Id1* induction in C2C12 myoblasts (Nofziger et al., 1999), again indicating that this role of PS1 is not operating through Notch signalling.

Several studies have reported that overexpression of PS1 alone is insufficient for enhancing γ-secretase activity, without concomitant overexpression of other members of the complex, including nicastrin, Aph-1 and Pen-2 (reviewed by De Strooper, 2003; Parks and Curtis, 2007; Vetrivel et al., 2006). Therefore, when we used expression vectors to constitutively express only PS1, γ-secretase activity should not have been enhanced. Indeed, myoblasts with constitutive expression of PS1 did not show altered levels of the ICD of either Notch1 or Notch2, or of Hes1 (Fig. 4I). However, to ensure that the effects of PS1 were uncoupled from any caused by increasing γ-secretase activity, we also employed, in parallel, potent inhibitors of γ-secretase activity (DAPT and L-685,458).

Constitutive expression of PS1 resulted in approximately fourfold more transfected satellite-cell-derived myoblasts with Pax7 protein than found in controls, and a significant inhibition of myogenic differentiation. Importantly, inhibiting γ-secretase activity with DAPT did not prevent these effects of constitutive PS1 expression, showing that PS1 acts independently of Notch signalling. Constitutive PS1 expression causes Id1 levels to be increased, presumably allowing more Id1 dimerisation with MyoD and inhibition of myogenic differentiation. Therefore, the failure of MyoD to induce Myog probably prevents the inhibition of Pax7 (Olguin et al., 2007).

We further explored the effects of PS1 on myogenesis using mouse cells with two null alleles of *PS1* (De Strooper et al., 1999; Herreman et al., 2000). *PS1*-null mice die in utero and so we examined MyoD-induced myogenesis in $PS1^{-/-}$ MEFs. Ectopic MyoD was able to efficiently induce myogenesis in $PS1^{-/-}$ MEFs maintained under high-serum conditions, and inhibition of γ-secretase activity with either DAPT or L-685,458 did not prevent this. By contrast, MyoD could not induce myogenesis under similar conditions in WT or $PS2^{-/-}$ MEFs (Fig. 7K), with or without concomitant γ-secretase inhibition. Because WT and $PS2^{-/-}$ MEFs had robust Id1 expression but $PS1^{-/-}$ MEFs did not, and co-transfection of MyoD with either PS1 or Id1 prevented myogenic differentiation of $PS1^{-/-}$ MEFs, these observations indicate that PS1, but not PS2, is able to prevent myogenesis by promoting Id1 function. We also independently confirmed that γ-secretase activity is not required for Id1 upregulation by PS1, by using a PS1 mutant that completely lacks γ-secretase activity (Tolia et al., 2006) yet still increases Id1 levels (Fig. 7).

We have recently shown that β-catenin, probably via canonical Wnt signalling, can influence satellite cell fate, with increased β-catenin levels promoting the self-renewal phenotype (Perez-Ruiz et al., 2008). Interestingly, it has been shown that PS1 can interact with various armadillo family members, including β-catenin (reviewed by Parks and Curtis, 2007; Vetrivel et al., 2006). PS1 binds β-catenin and can regulate β-catenin stability, in both positive and negative ways (Meredith et al., 2002; Vetrivel et al., 2006; Zhang et al., 1998). Specific inhibition of BMP signalling results in myogenic differentiation in high-serum culture conditions (Kodaira et al., 2006), and Id1 is a major effector of BMP signalling (Katagiri et al., 2002). We did not find any differences between WT and $PS1^{-/-}$ MEFs in the expression of proteins known to be upstream of Id1, such as pSmad1/5/8 and Egr-1 (our unpublished observations). Pharmacological blockade has shown that interactions between PS1 and β-catenin are independent of γ-secretase activity (Meredith et

al., 2002) and, as mentioned above, Notch ICD is not accompanied by *Id1* induction in C2C12 myoblasts (Nofziger et al., 1999). Thus, speculatively, PS1 might operate through its effects on β-catenin stability to affect canonical Wnt signalling to control Id1, independently of its γ-secretase activity.

PS1 is also known to regulate Ca^{2+} homeostasis through γ-secretase-independent mechanisms (Akbari et al., 2004; Tu et al., 2006). In regenerating muscles, Id1 can be negatively regulated by Calcineurin, a Ca^{2+}-calmodulin-dependent serine/threonine protein phosphatase (Sakuma et al., 2005), so PS1 might also control Id1 protein through the regulation of Ca^{2+} homeostasis. Id1 protein is also known to be controlled by protein stabilisation (Bounpheng et al., 1999), so PS1 might also more directly control Id1 expression through such a mechanism.

Taken together, our data provide evidence of a novel mechanism operating in stem cells, whereby PS1 controls Id1 to regulate the transcriptional activity of bHLH transcription factors, operating independently of γ-secretase activity. In the neural system for example, PS1 is essential for maintenance of the neural progenitor cell pool and for preventing neural differentiation in the developing brain (Hitoshi et al., 2002). In adults, proliferating neural progenitor cells strongly express PS1, but mature neurones do not (Wen et al., 2002). Importantly, Id1 negatively regulates neurogenic transcription factors such as Mash1 in brain (Nakashima et al., 2001; Vinals et al., 2004), paralleling its actions on MyoD in muscle. Speculatively therefore, PS1 might have a common role in maintaining the progenitor cell pool via regulation of Id1 in both muscle and brain. The demonstration of a PS1-Id1 signalling network might also provide new insight into the pathogenesis of mutated PS1-related early-onset familial Alzheimer's disease (reviewed by Parks and Curtis, 2007; Vetrivel et al., 2006).

In conclusion, our study shows that PS1 acts as a potent regulator of fate choice in muscle satellite cells. Undoubtedly, some of the effects of PS1 on satellite cell function are due to its role as a crucial component of the γ-secretase complex, central to Notch signalling. However, PS1 also operates in a γ-secretase-independent manner to control MyoD, and our results show that this is probably achieved through regulation of Id1. The mechanisms that promote satellite cell self-renewal for the maintenance of the stem cell pool and those that prevent precocious myogenic differentiation must be linked and feedback on each other to carefully regulate the extent of differentiation for repair, versus maintenance, of a viable stem cell pool, able to respond to future needs. PS1 control of MyoD transcriptional activity would appear to be one of these links between differentiation and self-renewal mechanisms.

Materials and Methods

Isolation and culture of primary satellite cells and myoblasts

Adult (8-12 weeks old) C57BL10 mice were killed by cervical dislocation, and the extensor digitorum longus (EDL) muscles isolated and digested in collagenase as previously described (Beauchamp et al., 2000). Myofibres and associated satellite cells were isolated and cultured in plating medium (DMEM supplemented with 10% horse serum, 0.5% chicken embryonic extract, 4 mM L-glutamine and 1% penicillin-streptomycin) at 37°C in 5% CO_2, as described previously (Perez-Ruiz et al., 2008). Satellite cells were removed from myofibres by enzymatic treatment with 0.125% trypsin-EDTA solution for 10 minutes at 37°C and maintained in high-serum-containing medium (DMEM supplemented with 20% FBS, 1% chicken embryo extract, 10 ng/ml FGF, 4 mM L-glutamine and 1% penicillin-streptomycin). This medium supported both proliferation and differentiation of satellite cell progeny when bFGF was removed. The C2 (Yaffe and Saxel, 1977) subclone C2C12 and 10T1/2 cell lines were obtained from Riken Cell Bank (Tsukuba, Japan). C2C12 cells were maintained in growth medium (GM; F-10 medium supplemented with 20% FBS and antibiotics). For myogenic differentiation (both C2 and satellite cells), the culture medium was replaced with differentiation medium (DM; DMEM containing 2% horse serum and antibiotics) for 72 hours at 37°C. 10T1/2 cells, WT, $PS1^{-/-}$, $PS2^{-/-}$, $PS1^{-/-}PS2^{-/-}$ MEFs and $PS1^{-/-}PS2^{-/-}$ MEFs expressing *Cys-less PS1* or *D385C PS1* (Herreman et al., 1999; Herreman et al., 2003) were maintained in DMEM containing 10% FBS and antibiotics.

Antibodies and Reagents

Antibodies were obtained from the following sources: mouse and rabbit anti-PS1 antibodies from Millipore (Bedford, MA); mouse anti-GFP from Roche (Basel, Switzerland); rabbit anti-PS2 antibody from Abcam; mouse anti-Notch1 antibody from BD Biosciences; rat anti-Ki67 from DAKO; goat anti-PS1 antibody, rabbit anti-Id1 antibody, rabbit anti-Hes1 antibody goat anti-Notch2 antibody and rabbit anti-MyoD antibody were obtained from Santa Cruz (Santa Cruz, CA); mouse anti-developmental myosin heavy chain (dMyHC) antibody from Novocastra (Newcastle, UK); mouse anti-MyHC (MF20), anti-Pax7 antibody, anti-Myog antibody (F5D) and anti-tubulin antibody (E7) were obtained from the DSHB (Iowa City, IA); rabbit anti-p-histone H3 antibody from Cell Signaling Technology (Beverly, MA) and Topro-3, rabbit anti-GFP antibody and mouse anti-V5 antibody from Invitrogen (Carlsbad, CA). Mounting medium containing DAPI was purchased from Vector Laboratories (Burlingame, CA). Nuclei were counterstained with either DAPI or Topro-3. DAPT and L-685,468 were purchased from Peptide Institute (Osaka, Japan) and dissolved and applied in DMSO. γ-secretase activity was measured using a γ-secretase activity detection kit according to the manufacturer's instructions (R&D Systems).

Immunoblot analysis

Immunoblot analysis was performed as previously described (Ono et al., 2006). Rabbit or mouse anti-PS1 (recognise loop domain), anti-PS2, anti-MyHC, anti-tubulin, anti-Pax7, anti-Notch1, anti-Notch2, anti-Hes1, anti-MyoD, anti-Id1 or anti-β-actin antibody were applied at 4°C overnight. Horseradish-peroxidase-conjugated secondary antibodies were used for visualisation by chemiluminescence with a digital luminescent image analyser LAS-1000 (Fujifilm, Tokyo, Japan).

Immunostaining

Immunocytochemistry was performed as previously described (Ono et al., 2007). Primary antibodies were used in PBS as follows: goat anti-PS1 (recognises N-terminal), anti-Id1, anti-Ki67, anti-MyHC, anti-Pax7, anti-Myog, mouse anti-GFP, rabbit anti-GFP, anti-V5 or anti-MyoD antibody at 4°C overnight. For immunohistochemistry, frozen muscle cross-sections were fixed with cold acetone, blocked with M.O.M kit (Vector Laboratories) and incubated with either anti-dMyHC or p-histone H3 antibody. Immunostained myofibres and plated cells were viewed on a Zeiss Axiophot 200M using Plan-Neofluar lenses, or on a Nikon C1si confocal using Plan-Fluor lenses. Digital images were acquired with a Zeiss AxioCam HRm Charge-Coupled Device using AxioVision software version 4.4. Images were optimised globally and assembled into figures using Adobe Photoshop.

RNA interference in vitro

The transfection of siRNA (Stealth siRNA; Invitrogen) into C2C12 myoblasts and primary muscle progenitors cells was performed using Lipofectamine 2000 reagent (Invitrogen) as previously described (Ono et al., 2007). Transfection of siRNA into single myofibres was carried out 20-24 hours after isolation. All samples were examined 72 hours after the transfection. The following siRNA sequences were used: *PS1* siRNA-1, 5′-ACTCTCTTTCCAGCTCTTATCTATT-3′; *PS1* siRNA-2, 5′-GCACCTTTGTCCTACTTCCAGAATG-3′; and *PS2* siRNA, 5′-CCACUAUCAA-GUCUGUGCGUUUCUA-3′. The control siRNA sequence and AlexaFlour488-conjugated siRNA were purchased from Invitrogen.

Plasmid construction and transfection

PS1 cDNA was cloned into *pMSCV-IRES-GFP* (Zammit et al., 2006) or *pCMV-V5*-expression vectors to generate *pMSCV-PS1-IRES-GFP* or *pCMV-PS1-V5* respectively. Transfection was performed once or twice (10 hours after the first transfection) using Lipofectamine 2000 (Invitrogen) or Lipofectamine LTX (Invitrogen) with Plus Reagents (Invitrogen) in accordance with the manufacturer's instructions.

Muscle injury and in vivo siRNA transfection

Male 8-week old C57BL/6N mice were used according to the Guidelines and Regulations for Laboratory Animal Care of Tohoku University Graduate School of Medicine. Muscle damage was induced by direct intramuscular injection of 50 μl of 10 μM cardiotoxin (Sigma) into the belly of gastrocnemius muscle using a 29G 1/2 insulin syringe. For in vivo siRNA transfection, siRNA duplexes were incubated with Atelocollagen (Koken, Japan) according to the manufacturer's instructions.

Statistical analysis

Data are presented as mean ± standard deviation. Comparisons among groups were determined by the Student's *t*-test. *P* values of <0.05 were considered to be statistically significant.

We would like to thank: Bart De Strooper (Center for Human Genetics, Katholieke Universiteit Leuven) for kindly providing the *Cys-less PS1* and *D385C PS1* constructs, and WT, $PS1^{-/-}$, $PS2^{-/-}$,

PS1$^{-/-}$*PS2*$^{-/-}$ MEFs and *PS1*$^{-/-}$*PS2*$^{-/-}$ MEFs expressing *Cys-less PS1* or *D385C PS1*; Douglas Melton and Robert Benezra for generously sharing constructs *pCMV-MyoD* and *pcDNA3-mId1*, respectively through Addgene; the Pax7, Myog, tubulin and MF20 antibodies, developed by A. Kawakami, W. E. Wright, M. Klymkowsky and D. A. Fischman, respectively, were obtained from the Developmental Studies Hybridoma Bank developed under the auspices of the NICHD and maintained by the University of Iowa; and Frederico Calhabeu and Paul Knopp for much help. Y.O. received support from Tohoku University research fellowships and is now funded by the Muscular Dystrophy Campaign (grant number RA3/737). V.F.G. is supported by the Medical Research Council (grant number G0700307). This work was supported in part by a research grant from the Uehara Memorial Foundation. The laboratory of P.S.Z. is also supported by the Association of International Cancer Research and the Wellcome Trust. Deposited in PMC for release after 6 months.

References

Akbari, Y., Hitt, B. D., Murphy, M. P., Dagher, N. N., Tseng, B. P., Green, K. N., Golde, T. E. and LaFerla, F. M. (2004). Presenilin regulates capacitative calcium entry dependently and independently of gamma-secretase activity. *Biochem. Biophys. Res. Commun.* **322**, 1145-1152.

Beauchamp, J. R., Heslop, L., Yu, D. S., Tajbakhsh, S., Kelly, R. G., Wernig, A., Buckingham, M. E., Partridge, T. A. and Zammit, P. S. (2000). Expression of CD34 and Myf5 defines the majority of quiescent adult skeletal muscle satellite cells. *J. Cell Biol.* **151**, 1221-1234.

Benezra, R., Davis, R. L., Lockshon, D., Turner, D. L. and Weintraub, H. (1990). The protein Id: a negative regulator of helix-loop-helix DNA binding proteins. *Cell* **61**, 49-59.

Bounpheng, M. A., Dimas, J. J., Dodds, S. G. and Christy, B. A. (1999). Degradation of Id proteins by the ubiquitin-proteasome pathway. *FASEB J.* **13**, 2257-2264.

Brack, A. S., Conboy, I. M., Conboy, M. J., Shen, J. and Rando, T. A. (2008). A temporal switch from notch to Wnt signaling in muscle stem cells is necessary for normal adult myogenesis. *Cell Stem Cell* **2**, 50-59.

Collins, C. A., Olsen, I., Zammit, P. S., Heslop, L., Petrie, A., Partridge, T. A. and Morgan, J. E. (2005). Stem cell function, self-renewal, and behavioral heterogeneity of cells from the adult muscle satellite cell niche. *Cell* **122**, 289-301.

Conboy, I. M. and Rando, T. A. (2002). The regulation of Notch signaling controls satellite cell activation and cell fate determination in postnatal myogenesis. *Dev. Cell* **3**, 397-409.

Conboy, I. M., Conboy, M. J., Smythe, G. M. and Rando, T. A. (2003). Notch-mediated restoration of regenerative potential to aged muscle. *Science* **302**, 1575-1577.

De Strooper, B. (2003). Aph-1, Pen-2, and Nicastrin with Presenilin generate an active gamma-Secretase complex. *Neuron* **38**, 9-12.

De Strooper, B., Annaert, W., Cupers, P., Saftig, P., Craessaerts, K., Mumm, J. S., Schroeter, E. H., Schrijvers, V., Wolfe, M. S., Ray, W. J. et al. (1999). A presenilin-1-dependent gamma-secretase-like protease mediates release of Notch intracellular domain. *Nature* **398**, 518-522.

Esselens, C., Oorschot, V., Baert, V., Raemaekers, T., Spittaels, K., Serneels, L., Zheng, H., Saftig, P., De Strooper, B., Klumperman, J. et al. (2004). Presenilin 1 mediates the turnover of telencephalin in hippocampal neurons via an autophagic degradative pathway. *J. Cell Biol.* **166**, 1041-1054.

Halevy, O., Piestun, Y., Allouh, M. Z., Rosser, B. W., Rinkevich, Y., Reshef, R., Rozenboim, I., Wleklinski-Lee, M. and Yablonka-Reuveni, Z. (2004). Pattern of Pax7 expression during myogenesis in the posthatch chicken establishes a model for satellite cell differentiation and renewal. *Dev. Dyn.* **231**, 489-502.

Hansson, E. M., Lendahl, U. and Chapman, G. (2004). Notch signaling in development and disease. *Semin. Cancer Biol.* **14**, 320-328.

Herreman, A., Hartmann, D., Annaert, W., Saftig, P., Craessaerts, K., Serneels, L., Umans, L., Schrijvers, V., Checler, F., Vanderstichele, H. et al. (1999). Presenilin 2 deficiency causes a mild pulmonary phenotype and no changes in amyloid precursor protein processing but enhances the embryonic lethal phenotype of presenilin 1 deficiency. *Proc. Natl. Acad. Sci. USA* **21**, 11872-11877.

Herreman, A., Serneels, L., Annaert, W., Collen, D., Schoonjans, L. and De Strooper, B. (2000). Total inactivation of gamma-secretase activity in presenilin-deficient embryonic stem cells. *Nat. Cell Biol.* **2**, 461-462.

Herreman, A., Van Gassen, G., Bentahir, M., Nyabi, O., Craessaerts, K., Mueller, U., Annaert, W. and De Strooper, B. (2003). gamma-Secretase activity requires the presenilin-dependent trafficking of nicastrin through the Golgi apparatus but not its complex glycosylation. *J. Cell Sci.* **116**, 1127-1136.

Hitoshi, S., Alexson, T., Tropepe, V., Donoviel, D., Elia, A. J., Nye, J. S., Conlon, R. A., Mak, T. W., Bernstein, A. and van der Kooy, D. (2002). Notch pathway molecules are essential for the maintenance, but not the generation, of mammalian neural stem cells. *Genes Dev.* **16**, 846-858.

Huppert, S. S., Ilagan, M. X., De Strooper, B. and Kopan, R. (2005). Analysis of Notch function in presomitic mesoderm suggests a gamma-secretase-independent role for presenilins in somite differentiation. *Dev. Cell* **8**, 677-688.

Jarriault, S., Brou, C., Logeat, F., Schroeter, E. H., Kopan, R. and Israel, A. (1995). Signalling downstream of activated mammalian Notch. *Nature* **377**, 355-358.

Jen, Y., Weintraub, H. and Benezra, R. (1992). Overexpression of Id protein inhibits the muscle differentiation program: in vivo association of Id with E2A proteins. *Genes Dev.* **6**, 1466-1479.

Jones, N. C., Tyner, K. J., Nibarger, L., Stanley, H. M., Cornelison, D. D., Fedorov, Y. V. and Olwin, B. B. (2005). The p38alpha/beta MAPK functions as a molecular switch to activate the quiescent satellite cell. *J. Cell Biol.* **169**, 105-116.

Katagiri, T., Imada, M., Yanai, T., Suda, T., Takahashi, N. and Kamijo, R. (2002). Identification of a BMP-responsive element in Id1, the gene for inhibition of myogenesis. *Genes Cells* **7**, 949-960.

Kinouchi, N., Ohsawa, Y., Ishimaru, N., Ohuchi, H., Sunada, Y., Hayashi, Y., Tanimoto, Y., Moriyama, K. and Noji, S. (2008). Atelocollagen-mediated local and systemic applications of myostatin-targeting siRNA increase skeletal muscle mass. *Gene Ther.* **15**, 1126-1130.

Kitzmann, M., Bonnieu, A., Duret, C., Vernus, B., Barro, M., Laoudj-Chenivesse, D., Verdi, J. M. and Carnac, G. (2006). Inhibition of Notch signaling induces myotube hypertrophy by recruiting a subpopulation of reserve cells. *J. Cell Physiol.* **208**, 538-548.

Kodaira, K., Imada, M., Goto, M., Tomoyasu, A., Fukuda, T., Kamijo, R., Suda, T., Higashio, K. and Katagiri, T. (2006). Purification and identification of a BMP-like factor from bovine serum. *Biochem. Biophys. Res. Commun.* **345**, 1224-1231.

Kopan, R., Nye, J. S. and Weintraub, H. (1994). The intracellular domain of mouse Notch: a constitutively activated repressor of myogenesis directed at the basic helix-loop-helix region of MyoD. *Development* **120**, 2385-2396.

Kuang, S., Kuroda, K., Le Grand, F. and Rudnicki, M. A. (2007). Asymmetric self-renewal and commitment of satellite stem cells in muscle. *Cell* **129**, 999-1010.

Lammich, S., Okochi, M., Takeda, M., Kaether, C., Capell, A., Zimmer, A. K., Edbauer, D., Walter, J., Steiner, H. and Haass, C. (2002). Presenilin-dependent intramembrane proteolysis of CD44 leads to the liberation of its intracellular domain and the secretion of an Abeta-like peptide. *J. Biol. Chem.* **277**, 44754-44759.

Lepper, C., Conway, S. J. and Fan, C. M. (2009). Adult satellite cells and embryonic muscle progenitors have distinct genetic requirements. *Nature* **460**, 627-631.

Mauro, A. (1961). Satellite cell of skeletal muscle fibers. *J. Biophys. Biochem. Cytol.* **9**, 493-495.

McKinnell, I. W., Ishibashi, J., Le Grand, F., Punch, V. G., Addicks, G. C., Greenblatt, J. F., Dilworth, F. J. and Rudnicki, M. A. (2008). Pax7 activates myogenic genes by recruitment of a histone methyltransferase complex. *Nat. Cell Biol.* **10**, 77-84.

Meredith, J. E., Jr., Wang, Q., Mitchell, T. J., Olson, R. E., Zaczek, R., Stern, A. M. and Seiffert, D. (2002). Gamma-secretase activity is not involved in presenilin-mediated regulation of beta-catenin. *Biochem. Biophys. Res. Commun.* **299**, 744-750.

Nagata, Y., Kobayashi, H., Umeda, M., Ohta, N., Kawashima, S., Zammit, P. S. and Matsuda, R. (2006a). Sphingomyelin levels in the plasma membrane correlate with the activation state of muscle satellite cells. *J. Histochem. Cytochem.* **54**, 375-384.

Nagata, Y., Partridge, T. A., Matsuda, R. and Zammit, P. S. (2006b). Entry of muscle satellite cells into the cell cycle requires sphingolipid signaling. *J. Cell Biol.* **174**, 245-253.

Nakashima, K., Takizawa, T., Ochiai, W., Yanagisawa, M., Hisatsune, T., Nakafuku, M., Miyazono, K., Kishimoto, T., Kageyama, R. and Taga, T. (2001). BMP2-mediated alteration in the developmental pathway of fetal mouse brain cells from neurogenesis to astrocytogenesis. *Proc. Natl. Acad. Sci. USA* **98**, 5868-5873.

Nofziger, D., Miyamoto, A., Lyons, K. M. and Weinmaster, G. (1999). Notch signaling imposes two distinct blocks in the differentiation of C2C12 myoblasts. *Development* **126**, 1689-1702.

Olguin, H. C., Yang, Z., Tapscott, S. J. and Olwin, B. B. (2007). Reciprocal inhibition between Pax7 and muscle regulatory factors modulates myogenic cell fate determination. *J. Cell Biol.* **177**, 769-779.

Ono, Y., Sensui, H., Sakamoto, Y. and Nagatomi, R. (2006). Knockdown of hypoxia-inducible factor-1alpha by siRNA inhibits C2C12 myoblast differentiation. *J. Cell Biochem.* **98**, 642-649.

Ono, Y., Sensui, H., Okutsu, S. and Nagatomi, R. (2007). Notch2 negatively regulates myofibroblastic differentiation of myoblasts. *J. Cell Physiol.* **210**, 358-369.

Parks, A. L. and Curtis, D. (2007). Presenilin diversifies its portfolio. *Trends Genet.* **23**, 140-150.

Perez-Ruiz, A., Ono, Y., Gnocchi, V. F. and Zammit, P. S. (2008). beta-Catenin promotes self-renewal of skeletal-muscle satellite cells. *J. Cell Sci.* **121**, 1373-1382.

Repetto, E., Yoon, I. S., Zheng, H. and Kang, D. E. (2007). Presenilin 1 regulates epidermal growth factor receptor turnover and signaling in the endosomal-lysosomal pathway. *J. Biol. Chem.* **282**, 31504-31516.

Sakuma, K., Nakao, R., Aoi, W., Inashima, S., Fujikawa, T., Hirata, M., Sano, M. and Yasuhara, M. (2005). Cyclosporin A treatment upregulates Id1 and Smad3 expression and delays skeletal muscle regeneration. *Acta Neuropathol.* **110**, 269-280.

Seale, P., Sabourin, L. A., Girgis-Gabardo, A., Mansouri, A., Gruss, P. and Rudnicki, M. A. (2000). Pax7 is required for the specification of myogenic satellite cells. *Cell* **102**, 777-786.

Shen, J., Bronson, R. T., Chen, D. F., Xia, W., Selkoe, D. J. and Tonegawa, S. (1997). Skeletal and CNS defects in Presenilin-1-deficient mice. *Cell* **89**, 629-639.

Skapek, S. X., Rhee, J., Kim, P. S., Novitch, B. G. and Lassar, A. B. (1996). Cyclin-mediated inhibition of muscle gene expression via a mechanism that is independent of pRB hyperphosphorylation. *Mol. Cell. Biol.* **16**, 7043-7053.

Struhl, G. and Greenwald, I. (1999). Presenilin is required for activity and nuclear access of Notch in Drosophila. *Nature* **398**, 522-525.

Tolia, A., Chavez-Gutierrez, L. and De Strooper, B. (2006). Contribution of presenilin transmembrane domains 6 and 7 to a water-containing cavity in the gamma-secretase complex. *J. Biol. Chem.* **281**, 27633-27642.

Tu, H., Nelson, O., Bezprozvanny, A., Wang, Z., Lee, S. F., Hao, Y. H., Serneels, L., De Strooper, B., Yu, G. and Bezprozvanny, I. (2006). Presenilins form ER Ca2+ leak channels, a function disrupted by familial Alzheimer's disease-linked mutations. *Cell* **126**, 981-993.

Vetrivel, K. S., Zhang, Y. W., Xu, H. and Thinakaran, G. (2006). Pathological and physiological functions of presenilins. *Mol Neurodegener.* **1**, 4.

Vinals, F., Reiriz, J., Ambrosio, S., Bartrons, R., Rosa, J. L. and Ventura, F. (2004). BMP-2 decreases Mash1 stability by increasing Id1 expression. *EMBO J.* **23**, 3527-3537.

Wen, P. H., Friedrich, V. L., Jr., Shioi, J., Robakis, N. K. and Elder, G. A. (2002). Presenilin-1 is expressed in neural progenitor cells in the hippocampus of adult mice. *Neurosci. Lett.* **318**, 53-56.

Wilson, C. A., Murphy, D. D., Giasson, B. I., Zhang, B., Trojanowski, J. Q. and Lee, V. M. (2004). Degradative organelles containing mislocalized alpha-and beta-synuclein proliferate in presenilin-1 null neurons. *J. Cell Biol.* **165**, 335-346.

Wong, P. C., Zheng, H., Chen, H., Becher, M. W., Sirinathsinghji, D. J., Trumbauer, M. E., Chen, H. Y., Price, D. L., Van der Ploeg, L. H. and Sisodia, S. S. (1997). Presenilin 1 is required for Notch1 and DII1 expression in the paraxial mesoderm. *Nature* **387**, 288-292.

Yaffe, D. and Saxel, O. (1977). Serial passaging and differentiation of myogenic cells isolated from dystrophic mouse muscle. *Nature* **270**, 725-727.

Yoshida, N., Yoshida, S., Koishi, K., Masuda, K. and Nabeshima, Y. (1998). Cell heterogeneity upon myogenic differentiation: down-regulation of MyoD and Myf-5 generates 'reserve cells'. *J. Cell Sci.* **111**, 769-779.

Zammit, P. S. (2008). All muscle satellite cells are equal, but are some more equal than others? *J. Cell Sci.* **121**, 2975-2982.

Zammit, P. S., Golding, J. P., Nagata, Y., Hudon, V., Partridge, T. A. and Beauchamp, J. R. (2004). Muscle satellite cells adopt divergent fates: a mechanism for self-renewal? *J. Cell Biol.* **166**, 347-357.

Zammit, P. S., Relaix, F., Nagata, Y., Ruiz, A. P., Collins, C. A., Partridge, T. A. and Beauchamp, J. R. (2006). Pax7 and myogenic progression in skeletal muscle satellite cells. *J. Cell Sci.* **119**, 1824-1832.

Zhang, Z., Hartmann, H., Do, V. M., Abramowski, D., Sturchler-Pierrat, C., Staufenbiel, M., Sommer, B., van de Wetering, M., Clevers, H., Saftig, P. et al. (1998). Destabilization of beta-catenin by mutations in presenilin-1 potentiates neuronal apoptosis. *Nature* **395**, 698-702.

Zhang, Z., Nadeau, P., Song, W., Donoviel, D., Yuan, M., Bernstein, A. and Yankner, B. A. (2000). Presenilins are required for gamma-secretase cleavage of beta-APP and transmembrane cleavage of Notch-1. *Nat. Cell Biol.* **2**, 463-465.

J Appl Physiol 107: 599–604, 2009.
First published June 18, 2009; doi:10.1152/japplphysiol.90821.2008.

Evaluation of individual skeletal muscle activity by glucose uptake during pedaling exercise at different workloads using positron emission tomography

Yuichi Gondoh,[1,2] Manabu Tashiro,[3] Masatoshi Itoh,[3] Mohammad M. Masud,[3] Hiroomi Sensui,[4] Shoichi Watanuki,[3] Kenji Ishii,[5] Hiroaki Takekura,[2] Ryoichi Nagatomi,[5] and Toshihiko Fujimoto[1]

[1]Center for Advancement of Higher Education, Tohoku University, Sendai; [2]Department of Physiological Sciences, National Institute of Fitness and Sports in Kanoya, Kagoshima; [3]Division of Cyclotron Nuclear Medicine, Cyclotron and Radioisotope Center, Tohoku University, Sendai; [4]Physical Fitness Research Institute, Meiji Yasuda Life Foundation of Health and Welfare, Tokyo; and [5]Department of Medicine and Science in Sports and Exercise, Graduate School of Medicine, Tohoku University, Sendai, Japan

Submitted 26 June 2008; accepted in final form 8 June 2009

Gondoh Y, Tashiro M, Itoh M, Masud MM, Sensui H, Watanuki S, Ishii K, Takekura H, Nagatomi R, Fujimoto T. Evaluation of individual skeletal muscle activity by glucose uptake during pedaling exercise at different workloads using positron emission tomography. *J Appl Physiol* 107: 599–604, 2009. First published June 18, 2009; doi:10.1152/japplphysiol.90821.2008.—Skeletal muscle glucose uptake closely reflects muscle activity at exercise intensity levels <55% of maximal oxygen consumption ($\dot{V}O_{2max}$). Our purpose was to evaluate individual skeletal muscle activity from glucose uptake in humans during pedaling exercise at different workloads by using [^{18}F]fluorodeoxyglucose (FDG) and positron emission tomography (PET). Twenty healthy male subjects were divided into two groups (7 exercise subjects and 13 control subjects). Exercise subjects were studied during 35 min of pedaling exercise at 40 and 55% $\dot{V}O_{2max}$ exercise intensities. FDG was injected 10 min after the start of exercise or after 20 min of rest. PET scanning of the whole body was conducted after completion of the exercise or rest period. In exercise subjects, mean FDG uptake [standardized uptake ratio (SUR)] of the iliacus muscle and muscles of the anterior part of the thigh was significantly greater than uptake in muscles of control subjects. At 55% $\dot{V}O_{2max}$ exercise, SURs of the iliacus muscle and thigh muscles, except for the rectus femoris, increased significantly compared with SURs at 40% $\dot{V}O_{2max}$ exercise. Our results are the first to clarify that the iliacus muscle, as well as the muscles of the anterior thigh, is the prime muscle used during pedaling exercise. In addition, the iliacus muscle and all muscles in the thigh, except for the rectus femoris, contribute when the workload of the pedaling exercise increases from 40 to 55% $\dot{V}O_{2max}$.

exercise intensity; fluorodeoxyglucose

EVALUATION OF INDIVIDUAL SKELETAL muscle activity during exercise or movement is an important physiological index for various aspects of not only sport medicine but also rehabilitation, medical engineering, and medical education. Electromyogram (EMG) is one way to measure muscle activity, but EMG is inadequate for measuring whole body muscle activity at one time. One of the reasons for the inadequacy of EMG is that it is difficult to use this method to measure the activity of muscles deep in the body, for example, the vastus intermedius, psoas major muscle, and iliacus muscle. The measurement of whole body muscle activity can provide important physiological information, because all types of exercise are achieved by a combination of muscle contractions. Richter et al. (22) reported that glucose disposal during exercise is dependent on power output and muscle mass recruited. Romijn et al. (23) also described that tissue uptake of plasma glucose increases in relation to exercise intensity. Our group (7) previously reported that glucose uptake of active skeletal muscle during pedaling exercise increased significantly from 30% of maximal oxygen consumption ($\dot{V}O_{2max}$) to 55% $\dot{V}O_{2max}$ intensity among untrained men. These results suggest that glucose uptake of skeletal muscle up to 55% $\dot{V}O_{2max}$ intensity closely reflected muscle activity. In addition, Pappas et al. (21) stated that [^{18}F]fluorodeoxyglucose (FDG) positron emission tomography (PET) successfully demonstrated increases in glucose consumption with increasing work production. Our group (5, 6, 25) reported on glucose uptake in individual skeletal muscles during aerobic running using PET. Similarly, Oi et al. (20) revealed lower extremity activity during level walking using PET. However, there are no reports observing individual skeletal muscle activities using PET during other sports or daily human activities. It is generally known that the quadriceps femoris muscle is the prime muscle during pedaling exercise, but details on the activities of other muscles, especially muscles deep in the body, are unknown.

In addition, previous studies have not demonstrated the effects of exercise intensity on the cooperative activity of individual skeletal muscles in the whole body. For example, the relative contribution of individual skeletal muscles during different levels of exercise intensity likely differs, even when the same exercise is being performed. Our group (7) observed that glucose uptake of muscles in the posterior part of thigh increased abruptly at high-intensity pedaling exercise compared with uptake at lower intensity exercise. This result indicated that the muscle activity of the posterior part of thigh would increase only at high intensity during pedaling exercise. However, there are no data regarding the relationship between individual muscle activities and exercise intensity on the whole body.

We hypothesized that muscles deep in the body might be activated during pedaling exercise and that the relative contribution of individual skeletal muscles during exercise might change when exercise intensity is increased. The purpose of the present investigation was to assess the muscle activities from the glucose uptake during pedaling exercise and to study the effect of exercise intensity (40 and 55% $\dot{V}O_{2max}$) on contributions of individual skeletal muscles for the exercise by using FDG and PET. Pedaling exercise was chosen because it is a

Address for reprint requests and other correspondence: T. Fujimoto, Center for the Advancement of Higher Education, Tohoku Univ., Kawauchi 41, Aoba-ku, Sendai 980-5876, Japan (e-mail: fujimoto@mail.tains.tohoku.ac.jp).

common daily movement and is also used worldwide for health promotion and various studies.

MATERIALS AND METHODS

Subjects. Twenty male subjects participated in this study. Subjects were healthy as judged by their medical history, physical examination, and routine laboratory tests. Subjects were randomly divided into two groups to limit the number exposed to the radioactive dosage of FDG: the exercise group (n = 7) and the control group (n = 13). The ethics committee of Tohoku University Graduate School of Medicine approved the study protocol. The purpose and potential risks were explained to all subjects, and written informed consent was received from all subjects before participation. The study was performed according to guidelines of the Declaration of Helsinki. The protocol of this study was approved by the ethics committee of Tohoku University Graduate School of Medicine, which is organized in accordance with the guidelines of the Ministry of Health, Labour, and Welfare of Japan.

Study protocol. Each exercise subject was studied on 2 separate days during a 3-wk period; study days were at least 2 days apart. All subjects could ride a bicycle, but they were not athlete cyclists. Subjects fasted for at least 6 h before the study, and any kind of strenuous physical activity was prohibited for at least 1 day before the experiment. Teflon catheters were inserted in the forearm antecubital veins for injection of FDG and arterialized venous blood samplings. Plasma glucose, serum insulin, and blood lactate samples were drawn immediately before and at the end of exercise. Exercise subjects cycled (828E ergometer; Monark, Varberg, Sweden) at intensities of 40 or 55% $\dot{V}O_{2max}$ at 60 revolutions per minute (rpm) without a toe clip. The seat height for each subject was set so that the angle of the subject's knee joint was about 10° when the pedal was at the bottom dead center of the crank cycle. The order of exercise intensity was randomized. Before the experiment, all subjects were requested to rest on a bed for 20 min. After 10 min of exercise, FDG (49.3 ± 1.2 and 39.5 ± 2.8 MBq for 40 and 55% $\dot{V}O_{2max}$ exercise, respectively) was injected, and thereafter the exercise continued for 25 min, for a total exercise time of 35 min. For the control group, FDG (46.8 ± 19.4 MBq) was injected after 20 min of rest, and subjects continued to rest for an additional 25 min. Fifteen minutes after the end of exercise or rest, a whole body three-dimensional (3-D) static emission scan was performed.

PET tracer, image acquisition, and processing. The synthesis of FDG was done using an automated method described previously (11, 17). The specific radioactivity of synthesized FDG was >37 MBq/μmol, and the radiochemical purity exceeded 98%.

PET (SET 2400W; Shimadzu, Kyoto, Japan) with an intrinsic spatial resolution of 3.9 mm full width at half maximum was used to create a PET scan constructed of 13 frames from the foot to the head (8). Each frame took 180 s for a total of 39 min. All PET data were corrected for dead time, decay, and photon attenuations. A whole body transmission scan was performed with a $^{68}Ge/^{68}Ga$ external rotating line source (370 MBq at purchase) maintaining similar procedures with PET emission scans. The axial field of view of the PET scanner was 200 mm. The image reconstruction was done by Tohoku University Supercomputer SX33 (NEC, Tokyo, Japan) through a 128 × 128 × 63 matrix for a set of 3-D volume images using a 3-D filtered back-projection algorithm (26).

Biochemical analysis. Measurements of glucose and lactate were done using the glucose oxidase method and a glucose analyzer (Gluco card GT-1630; KDK, Kyoto, Japan) and enzymatic lactate analyzer (Lactate Pro; KDK), respectively. In addition, serum insulin was measured using a double-antibody radioimmunoassay (Riabead 2; Dynabot, Tokyo, Japan; and γ coat cortisol; Incstar, Stillwater, MN).

Magnetic resonance imaging. After all PET scans, magnetic resonance imaging (MRI) scans were performed in anatomical locations similar to those of PET scans using the Spin Echo Sequence (Signa; GE Yokogawa, Tokyo, Japan) at 1.5 tesla. The measurement conditions were as follows: repetition time/echo time, 320/20 ms; number of excitations, 3; field of view, 45 cm; number of matrix, 256 × 256; slice thickness, 10 mm; and gap between slices, 0 mm.

Data analysis. To analyze the regions of interest (ROIs), we obtained tomographic images at the level of the planta, at the maximal girth of the leg (calf), at the midpoint of a line drawn between the patella and spina iliaca anterior superior (thigh), at the spina iliaca anterior superior (lower lumbar), at the 4th lumbar vertebra (upper lumbar), and at the 7th thoracic vertebra (chest). We measured FDG uptake in the 37 muscles in these regions. In addition, the location of individual skeletal muscles was confirmed by MRI (see Fig. 1*C*). To align the level in the PET image to the level in the MRI, we calculated the slice level from slice thickness and the slice number of each PET and MRI. These images were then displayed in isometry on the same screen. ROIs were drawn on PET images using image processing software (Dr. View; AJS, Tokyo, Japan).

The radioactivity from the ^{18}F atom of the FDG molecule trapped in the skeletal muscle tissue, measured in counts per second (cps) per unit, indicates the degree of glucose uptake per unit volume. The glucose uptake per unit volume of skeletal muscle (cps/pixel) is determined by the standardized uptake ratio (SUR) (18). Therefore, the glucose uptake by individual skeletal muscles for different exercise intensities (i.e., 40 and 55% $\dot{V}O_{2max}$) was evaluated using the SUR. This SUR is expressed by the following equation:

$$SUR = (a_{ROI} \cdot m)/[d \cdot f]$$

where a_{ROI} indicates the mean radioactivity count of the ROIs (cps/ml) of individual skeletal muscle, m indicates the total body weight in grams, d indicates the injected FDG dose, and f indicates the calibration factor. Detailed information is described in previous studies by our group (6, 25).

Exercise capacity. $\dot{V}O_{2max}$was determined using direct measurement of oxygen consumption rate (AE300-SRC; Minato, Tokyo, Japan) and a bicycle ergometer (Monark 818E) and was estimated using an incremental submaximal exercise test. Heart rate (HR) was monitored during exercise using a HR monitor (Vantage XL; Polar Electro, Kempele, Finland). The subjects cycled the bicycle ergometer at a pace of 60 rpm, with the load incrementally increased from 1 to 3 kp every 3 min. The estimated $\dot{V}O_{2max}$ was determined based on the relationships between HR-$\dot{V}O_{2max}$ and maximum HR (220 − age) (1).

Statistical analysis. All data are means ± SD. Statistical computations were performed with the SAS statistical program package (SAS Institute, Cary, NC). Student's t-test, Welch's t-test, or the Mann-Whitney U-test were used for analysis of statistical differences between the control group and exercise group at the intensity of 40% $\dot{V}O_{2max}$. The Mann-Whitney U-test (nonparametric analysis) was used when data did not have normality. The paired t-test or Wilcoxon signed-rank test was used for the analysis of statistical differences between the exercise group at 40 and 55% $\dot{V}O_{2max}$ intensities. An analysis of variance followed by the Bonferroni/Dunn test (1-factor ANOVA) was used to compare the SUR of individual muscles in the quadriceps femoris muscle. The paired t-test was used for the analysis of statistical differences between pre- and postrest or exercise values of blood glucose, serum insulin, and plasma lactate. The significant differences for all data were set at $P < 0.05$, $P < 0.01$ and $P < 0.001$.

RESULTS

There were no significant differences in individual physical characteristics between exercise and control subjects (Table 1). Figure 1*A* illustrates typical whole body PET images after exercise at 40 and 55% $\dot{V}O_{2max}$ intensity. Figure 2 shows the mean SURs of the muscles of control subjects and exercise subjects at 40 and 55% $\dot{V}O_{2max}$ exercise intensity. At 40% $\dot{V}O_{2max}$ exercise intensity, SURs of the skeletal muscles in the

Table 1. *Physical characteristics of subjects in each experimental group*

	Control Group	Exercise Group
No. of subjects	13	7
Age, yr	23.3±3.7	22.9±4.1
Weight, kg	61.9±6.7	61.1±7.5
Height, cm	170.4±4.7	172.0±4.0
Body mass index, kg/m^2	21.3±1.9	20.6±2.5
[$\dot{V}O_{2max}$], ml·kg^{-1}·min^{-1}	42.3±6.7	46.2±5.8

Values are means ± SD. [$\dot{V}O_{2max}$], maximal aerobic power.

lumbar region and anterior part of the thigh of exercise subjects were nearly two to five times higher than that of control subjects. Specifically, mean SURs of the iliacus, vastus lateralis, vastus intermedius, vastus medialis, and sartorius muscles at 40% $\dot{V}O_{2max}$ exercise intensity were more than 1.5, significantly higher than those of control subjects ($P < 0.05$, $P < 0.01$, or $P < 0.001$) (Fig. 2, *A* and *B*). SURs of the muscles in the lumbar region, posterior part of thigh, and below the knee joint also were relatively and significantly higher than those of control subjects ($P < 0.05$). Specifically, SURs of the psoas major, gracilis, adductor longus, adductor magnus, semimembranosus, semitendinosus, biceps femoris, rectus femoris, tibialis anterior, tibialis posterior, and extensor digitorum longus muscles were almost <1.0 but were significantly higher than that of control subjects.

At 55% $\dot{V}O_{2max}$ exercise intensity, SURs of the iliacus, vastus lateralis, vastus intermedius, vastus medialis, sartorius, biceps femoris, semitendinosus, semimembranosus, adductor magnus, adductor longus, and gracilis muscles increased significantly compared with SURs of those muscles at 40% $\dot{V}O_{2max}$ exercise intensity ($P < 0.05$, $P < 0.01$, or $P < 0.001$) (Fig. 2*C*). However, there were no significant increases in SURs of the psoas major, rectus femoris, tibialis anterior, tibialis posterior, and extensor digitorum longus muscles at 55% $\dot{V}O_{2max}$ compared with values at 40% $\dot{V}O_{2max}$ exercise intensity.

Figure 1, *B* and *C*, illustrates a typical PET image at the thigh level at both exercise intensities and an MRI obtained from the same region, respectively. The lower FDG uptake by the rectus femoris is shown in the PET image. The mean SURs of the rectus femoris were significantly lower than those of the vastus medialis and vastus intermedius at 40% $\dot{V}O_{2max}$ exercise intensity and significantly lower than those of the other three muscles of the quadriceps femoris muscle at 55% $\dot{V}O_{2max}$ exercise intensity ($P < 0.05$ or $P < 0.01$) (Fig. 2, *B* and *C*). In the control subjects, the mean SURs of rectus femoris were lower than those of the vastus medialis and vastus intermedius (Fig. 2*A*).

No changes were observed in plasma glucose concentrations in subjects during exercise at 40 or 55% $\dot{V}O_{2max}$ or in controls (Table 2). Compared with prerest or exercise values, serum insulin concentrations decreased slightly but significantly in the control group and the two exercise groups at postrest or exercise ($P < 0.05$). Plasma lactate concentrations remained unchanged during the control and exercise periods at 40% $\dot{V}O_{2max}$ intensity but increased significantly during intensity levels of 55% $\dot{V}O_{2max}$ ($P < 0.01$).

DISCUSSION

The purpose of the present investigation was to use FDG and PET to evaluate individual skeletal muscle activity based on glucose uptake during pedaling exercise at different workloads. FDG uptake of the iliacus muscle and the muscles in the anterior part of thigh was significantly higher in exercise

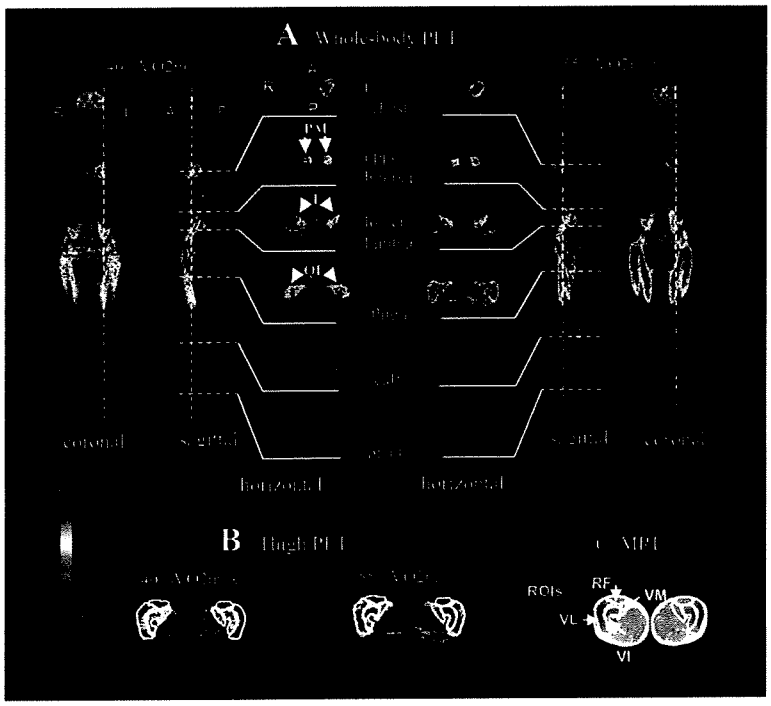

Fig. 1. Typical whole body PET images (*A*), typical PET images of the thigh region at 40 and 55% maximal oxygen consumption ($\dot{V}O_{2max}$) exercise intensity (*B*), and thigh MRI (*C*). Coronal PET images were obtained 144 mm anterior from the back. Sagittal images were obtained 68 mm left of the median line of body. Horizontal images were obtained from the appropriate plane as mentioned in MATERIALS AND METHODS. Dashed white lines show slice levels of coronal, sagittal, and horizontal scans. R, right; L, left; A, anterior; P, posterior; PM, psoas major muscle; I, iliacus muscle; QF, quadriceps femoris muscle; RF, rectus femoris muscle; VM, vastus medialis muscle; VI, vastus intermedius muscle; VL, vastus lateralis muscle. Regions of interest (ROIs) are represented by white lines on the thigh PET images and MRI scan. The red area at the center of the pelvis resulted from accumulation of [^{18}F]fluorodeoxyglucose (FDG) in the bladder.

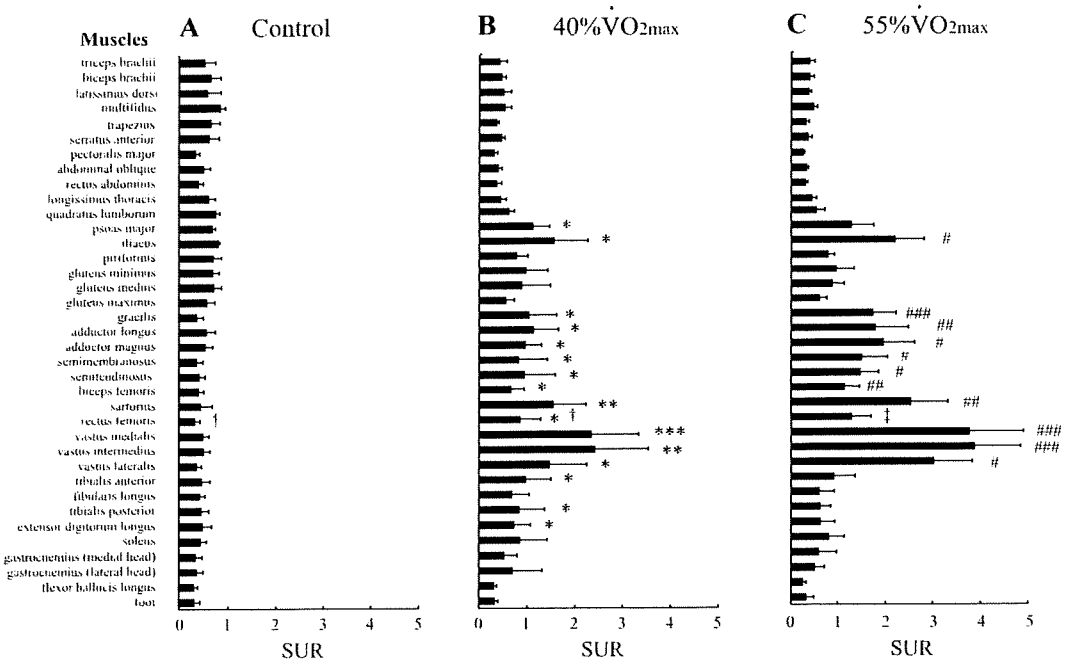

Fig. 2. Mean standardized uptake ratio (SUR) of the 37 muscles of control subjects (*A*), exercise subjects at 40% $\dot{V}O_{2max}$ (*B*), and exercise subjects at 55% $\dot{V}O_{2max}$ exercise intensity (*C*). Values are means ± SD. $*P < 0.05$; $**P < 0.01$; $***P < 0.001$ vs. control. $\#P < 0.05$; $\#\#P < 0.01$; $\#\#\#P < 0.001$ vs. 40% $\dot{V}O_{2max}$ intensity. $\dagger P < 0.05$ vs. VM and VI. $\ddagger P < 0.01$ vs. VL, VM, and VI.

subjects than control subjects. These results suggest that activities in the iliacus muscle and the muscles in the anterior part of the thigh increased during pedaling exercise. This is the first report that demonstrates increases in iliacus muscle activity during pedaling exercise.

Our group (7) previously reported that glucose uptake of skeletal muscle at up to 55% $\dot{V}O_{2max}$ intensity closely reflected muscle activity assessed by PET. Therefore, results of the present study imply that the iliacus muscle and the muscles in the anterior part of thigh are prime muscles for pedaling exercise. The iliacus muscle plays a role in hip-joint flexion, and muscles in the anterior part of the thigh function during knee-joint extension. During level walking and running, our previous results showed that the glucose uptake of the lower leg muscles was higher than that of the thigh muscles; however, the iliacus muscle did not have higher glucose uptake compared with the control state (6, 20). These results imply that pedaling exercise may be more useful for training the iliacus muscle than level walking and running. Because the iliacus muscle contributes to deep flexion of hip joint against the leg weight, this muscle plays an important role during step movements that occur in daily life. Whitt (27) has demonstrated that oxygen consumption for cycling at 12 miles/h (corresponding to active cycling speed in daily movement) with a touring (not racing) bicycle is 1.2 l/min. The oxygen consumption almost corresponds to 40% $\dot{V}O_{2max}$ of the present subjects of normal fitness level. In addition, 55% $\dot{V}O_{2max}$ of the present subjects (~1.55 l/min) corresponds to the oxygen consumption for cycling on a road with 1% rising gradient (existing everywhere) at the same speed (12 miles/h) with the same bicycle. These values mean that anyone has an opportunity to ride a bicycle in these work intensities in daily life and that riding a bicycle with this speed and gradient might be a better countermeasure to decrease the risk of falling accident than level walking and running. Therefore, compared with training by level walking and running, training by pedaling exercise might be a better countermeasure to decrease the risk of falling accident.

Glucose uptake of the psoas major muscle, muscles in the posterior part of the thigh, and some muscles of the leg below

Table 2. *Changes in circulating substrate concentrations in each experiment*

	Control		Exercise			
			40% [$\dot{V}O_{2max}$]		55% [$\dot{V}O_{2max}$]	
	Pre	Post	Pre	Post	Pre	Post
BG, mg/dl	92.6±7.7	91.2±10.9	100.1±10.9	94.1±12.4	99.3±8.5	95.4±11.7
SI, mU/l	5.4±3.0	4.3±1.9*	4.1±1.1	3.0±0.8*	4.4±1.5	2.0±0.6*
La, mM	1.1±0.2	1.0±0.2	1.0±0.4	1.1±0.2	0.9±0.2	4.1±2.1†

Values are means ± SD; $n = 13$ control subjects and 7 exercise subjects. Pre and post represent pre- and postrest values. BG, blood glucose level; SI, serum insulin level; La, plasma lactate level. $*P < 0.05$; $\dagger P < 0.01$ vs. Pre value in each experiment.

the knee joint also increased significantly at 40% $\dot{V}O_{2max}$ exercise intensity compared with those of control subjects. These results indicate that these muscles play important roles in pedaling exercise. The psoas major muscle plays a role in hip-joint flexion, and biceps femoris, semitendinosus, and semimembranosus hamstring muscles act during hip-joint extension. The adductor magnus, adductor, and gracilis muscles play a role in knee-joint extension and/or flexion during pedaling exercise. Leg muscles below the knee joint function with ankle joint extension and/or flexion. Takahashi et al. (24) clarified that the decline of the psoas major muscle starts at ages in the 20s and that in women, the decline in this muscle started earlier than the decline in the quadriceps femoris muscle. In addition, the decline of the psoas major muscle from ages in the 60s through the 70s was most remarkable. They also have shown that the psoas major muscle plays an important role in the walking ability of elderly persons and that declines in this muscle may contribute to falling. Therefore, falling accidents of elderly persons during walking may possibly be reduced by starting pedaling training early.

At 55% $\dot{V}O_{2max}$ exercise intensity, glucose uptake of the iliacus muscle and muscles in the thigh, except for the rectus femoris, increased significantly compared with those at 40% $\dot{V}O_{2max}$ exercise intensity ($P < 0.05$, $P < 0.01$, or $P < 0.001$). There was, however, no significant increase in glucose uptake of the psoas major, rectus femoris, and muscles of the leg below the knee joint at 55% $\dot{V}O_{2max}$ compared with those at 40% $\dot{V}O_{2max}$ exercise intensity. These results suggest that the activated muscles during pedaling exercise, with the exclusion of the psoas major, rectus femoris, and the muscles of the leg below the knee joint, contribute to the increase of workload from 40 to 55% $\dot{V}O_{2max}$. This result is also a novel finding in this study. The iliacus muscle and psoas major muscle are often considered a single muscle, referred to as the iliopsoas muscle. However, our results indicate that the iliacus muscle contributed to the increase of workload in the pedaling exercise more than the psoas major muscle.

This difference in function of the iliacus muscle and psoas major muscle might be caused by anatomical differences between these muscles. The iliacus muscle can directly affect the force to the thigh, since the iliacus muscle is a monoarticular muscle that crosses only the hip joint. However, the psoas major muscle is a multiarticular muscle that crosses the lumbar vertebrae joint and hip joint. For full multiarticular muscle activation, either the origin of the muscle or the insertion of the muscle, or both, must be fixed. The activity of the psoas major muscle during pedaling exercise at 55% also might be lower based on movement of the lumbar vertebrae joint due to the increase in exercise intensity; however, we cannot elucidate the clear cause of the difference in the activities of these muscles during different exercise intensities in this study.

Our results demonstrate that the activity of the rectus femoris is lower than that of other quadriceps femoris muscles during pedaling exercise. The glucose uptake of the rectus femoris muscle was significantly lower than that of the other three muscles in the quadriceps femoris muscle during pedaling exercise. In the control subjects, the glucose uptake of the rectus femoris muscle was lower than those of the vastus medialis and vastus intermedius muscle. The glucose uptake of skeletal muscle is affected by muscle fiber distribution. The vastus medialis muscle has a slightly higher number of type I fibers than rectus femoris muscle, but the vastus lateralis and rectus femoris muscle have a similar muscle fiber distribution (15). We do not have data on the muscle fiber distribution in vastus intermedius muscle. Therefore, the one of the causes of the difference in glucose uptake between vastus medialis muscle and rectus femoris muscle at pedaling exercise may be the slightly different muscle fiber distribution in this study. However, the differences in glucose uptake between vastus lateralis and rectus femoris muscle also cannot be explained solely by differences in muscle fiber distribution at 55% $\dot{V}O_{2max}$ intensity. Ericson et al. (4) reported that peak activity of the rectus femoris on the EMG was significantly lower than that of the vastus medialis and vastus intermedius during pedaling exercise. Endo et al. (3) also demonstrated the lower activity of the rectus femoris during pedaling exercise at some intensity, using MRIs. The data in our study correspond with their results.

This difference in function of the rectus femoris muscle and the other three muscles of quadriceps femoris muscle might be caused by anatomical differences between these muscles. The other three muscles can directly affect the force to the tibia, because they are monoarticular muscles, crossing only the knee joint. However, the rectus femoris muscle is a multiarticular muscle, crossing at the hip joint and knee joint. During pedaling exercise, the movement of hip joint and knee joint occur simultaneously. This simultaneous movement of two joints might explain the lower activity of the rectus femoris muscle during pedaling exercise at <55% $\dot{V}O_{2max}$ intensity.

Factors that influence the glucose uptake of skeletal muscles include muscle fiber distribution (12–14), muscle activity, defined as the power output, plasma glucose levels, and insulin concentrations. However, the large differences in glucose uptake among the muscles noted in this study cannot be explained only by differences in muscle fiber distribution as described in previous studies (7, 16). A previous study demonstrated that the difference in muscle fiber distribution is observed in many muscles (15). However, the percentage difference between type I fibers and type II fibers is <20% in most muscles with the exception of a few, such as the soleus and tibialis anterior. Gaster et al. (10) reported that the difference in density of glucose transporter 4 between slow fibers and fast fibers was ~12% in young subjects. Thus the big differences in SUR among the muscles in this study cannot be explained solely by differences in muscle fiber distribution. Although the blood flow in muscle is thought to be one factor that affects glucose uptake by muscles (2), one study (19) strongly supported the idea that glucose and FDG uptake are not regulated by blood flow. In the present study, blood glucose concentrations did not change, and the serum insulin concentrations decreased significantly in the control and exercise groups. These results suggest that changes in serum insulin levels did not influence FDG uptake in this study.

Currently, PET scanning during dynamic exercise is technically problematic. Therefore, the injection of FDG as used in the present study was performed during exercise, which was then continued for an additional 25 min, and scanning was performed after exercise. Despite this, the measured glucose uptake values reflect actual glucose uptake during exercise. After phosphorylation, the glucose analog (FDG) is trapped inside the muscle cell where further metabolism is prevented due to its chemical characteristics. This metabolic state of

phosphorylated FDG is preserved for ~2 h after injection (9). Plasma radioactivity peaked shortly after FDG injection and then decreased quickly during exercise (16). In addition to the tissue glucose uptake, the total uptake of tracer into the tissues is dependent on the availability of the tracer.

In this study, subjects were not bicycle race athletes, and we used a touring (not racing) bicycle ergometer. Therefore, the results of this study demonstrate muscle activities representative of subjects who have ordinary pedaling skills. Results might be different among bicycle race athletes, who have a higher level of pedaling skills.

One limitation of this study was the use of a separate control and exercise group as opposed to a crossover design. This was done to limit the radioactive dosage for each subject much as possible, based on the recommendations of the ethical committee of Tohoku University Graduate School of Medicine.

In conclusion, results of this study suggest that the activity of the iliacus muscle and muscles of the anterior part of thigh were critical during the pedaling exercise. The muscles in the posterior part of the thigh are important for pedaling exercise, although activation levels are lower than for the iliacus muscle and muscles of the anterior part of thigh. In addition, the iliacus muscle and all muscles in the thigh, with the exception of the rectus femoris and psoas major muscle, contribute to increasing workload of pedaling exercise from 40 to 55% $\dot{V}O_{2max}$ intensity.

ACKNOWLEDGMENTS

We thank Prof. Shin Fukudo of Tohoku University School of Medicine, Dr. Tetsuo Takaishi of Nagoya City University, and Dr. Hiroyuki Shimada of the Tokyo Metropolitan Institute of Gerontology for constructive comments. All staffs of the Cyclotron and Radioisotope Center, Tohoku University, are acknowledged for skillful assistance in performing PET scanning.

GRANTS

This work was supported in part by Grant-in-Aid 14704059 (to T. Fujimoto) from the Ministry of Education, Culture, Sports, Science and Technology of Japan and the Japan Science and Technology Agency, as well as a grant from the Japan Society of Technology on research and education in "molecular imaging." This work was also supported by the 12th Research Grant in Medical and Health Science of Meiji Yasuda Life Foundation of Health and Welfare.

REFERENCES

1. **Astrand P, Rhyming I.** A nomogram for calculation of aerobic capacity (physical fitness) for pulse rate during submaximal work. *J Appl Physiol* 7: 218–221, 1954.
2. **DeFronzo RA, Ferrannini E, Sato Y, Felig P, Wahren J.** Synergistic interaction between exercise and insulin on peripheral glucose uptake. *J Clin Invest* 68: 1468–1474, 1981.
3. **Endo MY, Kobayakawa M, Kinugasa R, Kuno S, Akima H, Rossiter HB, Miura A, Fukuba Y.** Thigh muscle activation distribution and pulmonary $\dot{V}O_2$ kinetics during moderate, heavy, and very heavy intensity cycling exercise in humans. *Am J Physiol Regul Integr Comp Physiol* 293: R812–R820, 2007.
4. **Ericson MO, Nisell R, Arborelius UP, Ekholm J.** Muscular activity during ergometer cycling. *Scand J Rehabil Med* 17: 53–61, 1985.
5. **Fujimoto T, Itoh M, Kumano H, Tashiro M, Ido T.** Whole-body metabolic map with positron emission tomography of a man after running. *Lancet* 348: 266, 1996.
6. **Fujimoto T, Itoh M, Tashiro M, Yamaguchi K, Kubota K, Ohmori H.** Glucose uptake by individual skeletal muscles during running using whole-body positron emission tomography. *Eur J Appl Physiol* 83: 297–302, 2000.
7. **Fujimoto T, Kemppainen J, Kalliokoski KK, Nuutila P, Ito M, Knuuti J.** Skeletal muscle glucose uptake response to exercise in trained and untrained men. *Med Sci Sports Exerc* 35: 777–783, 2003.
8. **Fujiwara T, Watanuki S, Yamamoto S, Miyake M, Seo S, Itoh M, Ishii K, Orihara H, Fukuda H, Satoh T, Kitamura K, Tanaka K, Takahashi S.** Performance evaluation of a large axial field-of-view PET scanner: SET-2400W. *Ann Nucl Med* 11: 307–313, 1997.
9. **Gallagher BM, Ansari A, Atkins H, Casella V, Christman DR, Fowler JS, Ido T, MacGregor RR, Som P, Wan CN, Wolf AP, Kuhl DE, Reivich M.** Radiopharmaceuticals XXVII. ^{18}F-labeled 2-deoxy-2-fluoro-D-glucose as a radiopharmaceutical for measuring regional myocardial glucose metabolism in vivo: tissue distribution and imaging studies in animals. *J Nucl Med* 18: 990–996, 1977.
10. **Gaster M, Poulsen P, Handberg A, Schroder HD, Beck-Nielsen H.** Direct evidence of fiber type-dependent GLUT-4 expression in human skeletal muscle. *Am J Physiol Endocrinol Metab* 278: E910–E916, 2000.
11. **Hamacher K, Coenen HH, Stöcklin G.** Efficient stereospecific synthesis of NO-carrier-added 2-[^{18}F]-fluoro-2-deoxy-D-glucose using aminopolyether supported nucleophilic substitution. *J Nucl Med* 27: 235–238, 1986.
12. **Hardin DS, Azzarelli B, Edwards J, Wigglesworth J, Maianu L, Brechtel G, Johnson A, Baron A, Garvey WT.** Mechanisms of enhanced insulin sensitivity in endurance-trained athletes: effects on blood flow and differential expression of GLUT 4 in skeletal muscles. *J Clin Endocrinol Metab* 80: 2437–2446, 1995.
13. **Hardin DS, Dominguez JH, Garvey WT.** Muscle group-specific regulation of GLUT 4 glucose transporters in control, diabetic, and insulin-treated diabetic rats. *Metabolism* 42: 1310–1315, 1993.
14. **Henriksen EJ, Bourey RE, Rodnick KJ, Koranyi L, Permutt MA, Holoszy JO.** Glucose transporter protein content and glucose transport capacity in rat skeletal muscles. *Am J Physiol Endocrinol Metab* 259: E593–E598, 1990.
15. **Johnson MA, Polgar J, Weightman D, Appleton D.** Data on the distribution of fibre types in thirty-six human muscles. An autopsy study. *J Neurol Sci* 18: 111–129, 1973.
16. **Kemppainen J, Fujimoto T, Kalliokoski KK, Viljanen T, Nuutila P, Knuuti J.** Myocardial and skeletal muscle glucose uptake during exercise in humans. *J Physiol* 542: 403–412, 2002.
17. **Kilbourn MR, Hood JT, Welch MJ.** A simple ^{18}O water target for ^{18}F production. *Int J Appl Radiat Isot* 35: 599–602, 1984.
18. **Kubota K, Matsuzawa T, Ito M, Ito K, Fujiwara T, Abe Y, Yoshioka S, Fukuda H, Hatazawa J, Iwata R, Watanuki S, Ido T.** Lung tumor imaging by positron emission tomography using C-11 L-methionine. *J Nucl Med* 26: 37–42, 1985.
19. **Nuutila P, Raitakari M, Laine H, Kirvelä O, Takala T, Utriainen T, Mäkimattila S, Pitkänen OP, Ruotsalainen U, Iida H, Knuuti J, Yki-Järvinen H.** Role of blood flow in regulating insulin-stimulated glucose uptake in humans. Studies using bradykinin, [^{15}O]water, and [^{18}F]fluoro-deoxy-glucose and positron emission tomography. *J Clin Invest* 97: 1741–1747, 1996.
20. **Oi N, Iwaya T, Itoh M, Yamaguchi K, Tobimatsu Y, Fujimoto T.** FDG-PET imaging of lower extremity muscular activity during level walking. *J Orthop Sci* 8: 55–61, 2003.
21. **Pappas GP, Olcott EW, Drace JE.** Imaging of skeletal muscle function using ^{18}FDG PET: force production, activation, and metabolism. *J Appl Physiol* 90: 329–337, 2001.
22. **Richter EA, Ruderman NB, Schneider SH.** Diabetes and exercise. *Am J Med* 70: 201–209, 1981.
23. **Romijn JA, Coyle EF, Sidossis LS, Gastaldelli A, Horowitz JF, Endert E, Wolfe RR.** Regulation of endogenous fat and carbohydrate metabolism in relation to exercise intensity and duration. *Am J Physiol Endocrinol Metab* 265: E380–E391, 1993.
24. **Takahashi K, Takahashi HE, Nakadaira H, Yamamoto M.** Different changes of quantity due to aging in the psoas major and quadriceps femoris muscles in women. *J Musculoskelet Neuronal Interact* 6: 201–205, 2006.
25. **Tashiro M, Fujimoto T, Itoh M, Kubota K, Fujiwara T, Miyake M, Watanuki S, Horikawa E, Sasaki H, Ido T.** ^{18}F-FDG PET imaging of muscle activity in runners. *J Nucl Med* 40: 70–76, 1999.
26. **Townsend DW, Defrise M, Geissbuhler A, Spinks TJ, Bailey DL, Gilardi MC, Jones T.** Normalisation and reconstruction of PET data acquired by a multi-ring camera with septa retracted. *Med Prog Technol* 17: 223–228, 1991.
27. **Whitt FR.** A note on the estimation of the energy expenditure of sporting cyclists. *Ergonomics* 14: 419–424, 1971.

Brain, Behavior, and Immunity 23 (2009) 108–115

Contents lists available at ScienceDirect

Brain, Behavior, and Immunity

journal homepage: www.elsevier.com/locate/ybrbi

Acute stress-induced colonic tissue HSP70 expression requires commensal bacterial components and intrinsic glucocorticoid

Kaori Matsuo [a], Xiumin Zhang [b], Yusuke Ono [c], Ryoichi Nagatomi [a,*]

[a] Department of Medicine and Science in Sports and Exercise, Tohoku University Graduate School of Medicine, 2-1 Seiryo-machi, Aoba-ku, Sendai, Japan
[b] School of Public Health, Jilin University, China
[c] Randall Division of Cell and Molecular Biophysics, King's College London, London, UK

ARTICLE INFO

Article history:
Received 1 May 2008
Received in revised form 22 July 2008
Accepted 29 July 2008
Available online 11 September 2008

Keywords:
HSP70
ZO-1
Acute restraint stress
Commensal bacteria
TLR4

ABSTRACT

Induction of heat shock protein (HSPs) has a protective effect in cells under stress. Physical stressors, such as restraint, induce HSPs in colonic tissue *in vivo*, but the mechanism of HSP induction is not yet clear. Because commensal bacteria support basal expression of colon epithelial HSP70, we postulated that stress responses may enhance the interaction of commensal bacteria and the colonic tissue. Restraining C57BL/6 mice for 2 h effectively induced HSP70 in colonic epithelia. Both blockade of stress-induced glucocorticoid by RU486 or elimination of commensal bacteria by antibiotics independently abrogated restraint-induced HSP70 augmentation. Oral administration of LPS to commensal-depleted mice restored restraint-induced HSP70 augmentation. Because TLR4 expression was absent from the epithelial surface, and was limited to lamina propria and muscularis externa, we examined how LPS reaches the lamina propria. Alexa-LPS administered in the colonic lumen was only detected in the lamina propria of the restrained mice. Expression of the tight junction component ZO-1 in the epithelia, which regulates the passage of luminal substances through the epithelia, was reduced after restraint, but reversed by RU486.

In conclusion, HSP70 induction in colonic epithelial cells under restraint requires both stress-induced glucocorticoid and luminal commensal bacteria, and LPS plays a significant role. Glucocorticoid-dependent attenuation of epithelial tight junction integrity may facilitate the access of LPS into the lamina propria, where TLR4, known to be required for HSP70 induction, is abundantly expressed. Sophisticated regulation of colonic protection against stressors involving the general stress response and the luminal environment has been demonstrated.

1. Introduction

Stress episodes are important risk factors for the development and reactivation of intestinal inflammation in rodents (Qiu et al., 1999) and in humans (Levenstein et al., 2000; Stam et al., 1997). Both environmental and psychological stress are known to alter the clinical course of inflammatory bowel disease (IBD) (Danese et al., 2004; Kugathasan et al., 2007; Mawdsley and Rampton, 2005; Tanaka et al., 2007; Tlaskalova-Hogenova et al., 2004). General stress reactions, such as activation of the HPA axis upon acute stress, are commonly accepted as having protective effects (Ader et al., 1979; Besedovsky and Sorkin, 1977; Riley, 1981). However, it has not been well documented how such adaptational reactions occur or are disrupted in the colon.

One of the cellular protective measures against stressors is the induction of HSP expression. HSPs are highly conserved proteins found in all prokaryotes and eukaryotes (Tobian et al., 2004). HSPs serve as molecular chaperones and play a significant role in the protection of cells against various cellular stressors, such as heat (Cvoro et al., 1998; Evdonin et al., 2006; Tomasovic et al., 1983), hypoxia (Dwyer et al., 1989; Zimmerman et al., 1991), ultraviolet irradiation (Kwon et al., 2002; Trautinger et al., 1996), oxidative stress (Drummond and Steinhardt, 1987), or endoplasmic reticulum stress (Yoneda et al., 2004). Unless intracellular HSPs are induced to protect cells exposed to acute stressors, they may undergo apoptosis or necrosis (Yun et al., 1997).

HSPs are also induced in various tissues and organs in response to various psychophysiological stressors (Fleshner et al., 2004; Fukudo et al., 1997), such as restraint (Campisi et al., 2003), ischemia (Kukreja et al., 1994; Lee et al., 2006; Oksala et al., 2002), exercise (Fehrenbach et al., 2005), infection (Ramaglia et al., 2004), inflammation (Ludwig et al., 1999), and hyperthermia (Hotchkiss et al., 1993). Among the various HSPs, HSP70[1] has recently been shown

* Corresponding author. Fax: +81 22 7178589.
E-mail address: nagatomi@m.tains.tohoku.ac.jp (R. Nagatomi).

[1] *Abbreviations used:* HSP70, heat shock protein 70; ZO-1,zonula occludens-1; TLR4, Toll-like receptor 4; RU486, mifepristone; LPS, lipopolysaccharide; ELISA, enzyme-linked immunosorbent assay.

0889-1591/$ - see front matter © 2008 Elsevier Inc. All rights reserved.
doi:10.1016/j.bbi.2008.07.013